Priest Lake Water Resources

Investigating the Influence of Spatiotemporal Ice Coverage Trends on Water Temperature in Priest Lake

Summer 2025 | Virginia – Langley
August 8th, 2025

Authors: Emma Skelton (Analytical Mechanics Associates), ErinGrace Drake (Analytical Mechanics Associates), Henry Osei (Analytical Mechanics Associates), John Nkrumah Mensah (Analytical Mechanics Associates)

Abstract:
Lakes around the globe are experiencing an increase in water temperature resulting in changes to lacustrine ecological systems. Priest Lake in Northern Idaho is thought to be experiencing these warming effects which in turn would have an impact on the winter ice duration and fisheries downstream in Priest River. The Idaho Conservation League, USGS Forest and Rangeland Ecosystem Science Center, Kalispel Tribe of Indians, and the Selkirk Conservation Alliance all hold a stake in the health of Priest Lake. These organizations take a multi-faceted approach to decision making for watershed management by working to include community members, local stakeholders, and technical experts in evaluation of changing conditions. Limited long-term water surface temperature and ice phenology data presented a challenge for evaluating warming trends in Priest Lake. This study used a combination of multispectral and synthetic aperture radar imagery to analyze trends in water surface temperature and ice presence from 1990 to 2024 on three areas of interest: Priest Lake, Upper Priest Lake, and the Outlet Bay. Results indicated a general increasing trend in water surface temperature along with a delay in ice-on date with a probability analysis suggesting a decrease in the likelihood of ice formation in November and December. Correlation analysis between maximum summer water surface temperature and ice-on date revealed a minimal relationship between lake temperature and ice phenology. Although these results align with global trends, cloud coverage, wind disturbances, and limited data impacted analysis and results. This highlights the feasibility of using Earth observations, demonstrating a need for more local observations to verify findings.

Key Terms: ice coverage, water resources, Priest Lake, SAR, Landsat, ice phenology, water surface temperature

Advisors: Benjamin Holt (California Institute of Technology, Jet Propulsion Laboratory), Manu Tom (California Institute of Technology, Jet Propulsion Laboratory), Dr. Kenton Ross (National Aeronautics and Space Administration)

Lead: Gwenyth Greco (California – JPL)

1. Introduction

1.1 Background Information

In temperate regions, most lakes are inhabited by cold-water fish species such as salmon and trout, which thrive in cooler water temperatures (10-18 °C). However, in recent years, the global water temperature has changed dramatically with a recent projected increase of 0.34°C per decade (O'Reilly et al., 2015). Recent increasing surface (land and water) temperatures are associated with the exacerbation of warming lake temperatures (Calvin et al., 2023). For cold-water fish populations, ice phenology (ice-on, ice off, duration) is critical for aquatic ecological processes and organismal survival and reproduction. In the past 25 years, lake ice-on has been increasingly delayed while lake ice-off has accelerated (Sharma et al., 2021). These changes contribute to the recent decline of cold-water fish population across the globe (Xu et al., 2024). Threatened fish populations have caused a more drastic need to monitor water temperature and devise appropriate measures to restore habitat (Mejia et al., 2021).

Priest Lake, part of the Priest River watershed in Northern Idaho (Figure 1), is affected by this impending change (Sharma et al., 2021). Reduced ice coverage and warming waters of Priest Lake and Upper Priest Lake pose a threat to native cold-water fish living in the downstream Priest River (Mejia et al., 2021). Thus, the assessment of ice phenology and its relation to surface water temperature is necessary to evaluate shifting thermal patterns which can have drastic impacts on lake ecosystems, leading to shorter winters and less ice cover (Culpepper et al., 2025; Piccolroaz et al., 2024). Understanding how to best monitor the lake is a priority for the Idaho Conservation League (ICL) and the United States Geological Survey (USGS) Forest and Rangeland Ecosystem Science Center, alongside local stakeholders, including representatives from the Kalispel Tribe of Nations, Natural Resources Department, and the Selkirk Conservation Alliance. The ICL works to protect clean air and water across Idaho through a multifaceted approach that combines community input, collaboration with diverse stakeholders, and enhanced data analysis with limited remote sensing. Field information on ice freeze and break-up in Priest Lake is limited due to financial and time constraints, as well as there being some complexities with identifying this transient stage. DEVELOP partnered with these organizations to assess the feasibility of using Earth observations to evaluate changing conditions. Earth observations can be used to evaluate surface water temperature where direct measurements are limited or unavailable.

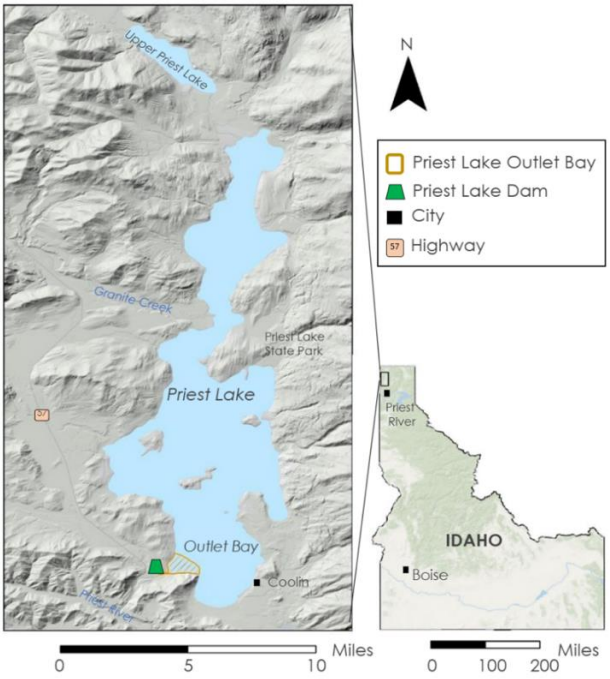

[Basemap Credit: ESRI, Garmin, NaturalVue, NOAA OCS]

Figure 1. Study area map of Priest Lake, Upper Priest Lake, and other essential parts to the watershed.

Remote sensing methods for lake ice detection and surface water temperature are an effective way to capture long-term trends with readily available data. Optical remote sensing methods are used to detect lake ice by leveraging the differences in reflective properties between water and ice. Prior studies have evaluated lake ice coverage by using indices and thresholds to identify water, ice, and snow. Sojka et al. (2023) used the Normalized Difference Water Index (NDWI), the Normalized Difference Snow Index (NDSI) and a threshold of the blue spectral band from Landsat to assess variability in ice cover on Polish lakes. Landsat thermal bands have been used to efficiently extract surface temperature data (Korver et al., 2024). Synthetic aperture radar (SAR) data are particularly valuable for monitoring lake ice, as they provide insights into the ice structural composition and allow for consistent observations regardless of weather conditions, including cloud cover. For instance, Murfitt & Dugay (2020) utilized Sentinel-1 C-SAR data to characterize ice phenology for Lake Hanzen in Nunavut, Canada. Shaposhnikova et al. (2023) supplemented Sentinel-1 data with RADARSAT and the European Remote-Sensing Satellites to evaluate lake ice in Old Crow Flats, Canada.

This study evaluated the feasibility of utilizing Earth observations to assess spatiotemporal trends of ice phenology, coverage, and their relation to lake surface temperature between the years 1990 - 2024 across Priest Lake. To support the partners in their decision-making process, this study looked to complete three main objectives: data collection from earth observations, evaluation of temporal trends in ice phenology, and correlation analysis between ice coverage and surface water temperature. Trends in lake ice coverage and extent were evaluated only for the winter months, using a combination of active and passive remote sensing methods. Remote sensing data supplemented direct water temperature measurements from the USGS, Kalispel Tribe, and the Selkirk Conservation Alliance. Results from this work will allow the partners to advocate for watershed management strategies that adapt to changing conditions.

2. Methodology

2.1 Data Acquisition

2.1.1 Multispectral Data Acquisition

This study used publicly available optical imagery to analyze water surface temperature and assess ice coverage. Data was downloaded from USGS Earth Explorer from the Landsat Collection 2 Level 1 and 2 products for the scene ID 043026, which includes both Upper Priest Lake and Priest Lake. To minimize atmospheric interference, this study acquired only images with ≤ 70% cloud coverage. As this study was multi-decadal, it required the use of both Landsat 4-5 Thematic Mapper (1990–2013) and Landsat 8-9 Operational Land Imager 1 & 2 and Thermal Infrared Sensor 1& 2 (2013–2024) (Table 1). Thermal bands were used to investigate water surface temperature and were acquired for all months of the study period. Additionally, the quality assurance (QA*)* band was acquired for each scene to implement cloud masking. For assessing ice coverage, panchromatic, green, near infrared (NIR), and short-wave infrared 1 (SWIR-1) bands were obtained from November to April. The spatial resolution for all the bands is 30 meters, except the thermal band of Landsat 4-5 which is 120 meters, the thermal band of Landsat 8-9 which is 100 meters and the panchromatic band of Landsat 8-9 which is 15 meters.

Table 1
Optical Data Acquired from USGS Earth Explorer

Product	Sensor	Collection	Bands
Surface Temperature	Landsat 8-9 OLI/TIRS	Landsat Collection 2 Level 2	B10 (Thermal Infrared-1)
	Landsat 4-5 TM		B6 (Thermal)
Surface Reflectance	Landsat 8-9 OLI/TIRS	Landsat Collection 2 Level 1	B8 (Panchromatic)
		Landsat Collection 2 Level 2	B3 (Green), B5 (NIR), B6 (SWIR-1
	Landsat 4-5 TM	Landsat Collection 2 Level 2	B2 (Green), B4 (NIR), B5 (SWIR-1)

2.1.2 SAR Data Acquisition

Radar imagery was acquired from multiple SAR missions and data providers to cover the entire study period. The platforms used include Sentinel-1, European Remote Sensing Satellite (ERS) 1 & 2, Envisat, RADARSAT-1, and Advanced Land Observing Satellite Phased Array L-band Synthetic Aperture Radar (ALOS PALSAR). Each of these platforms covered a specific time frame of the study period and had minimal overlap with one another (Table 2). All datasets were acquired in the C-band wavelength, except for ALOS PALSAR, which used the L-band. Depending on platform specifications and availability, radar data was filtered by polarization, including VV (Vertical-Vertical), VH (Vertical-Horizontal), HV (Horizontal-Vertical), and HH (Horizontal-Horizontal).

Table 2
Acquired SAR Data

Sensor	Polarization	Source	Spatial Resolution (range × azimuth)	Temporal Coverage
Sentinel-1 C-Band	VV and VH	Google Earth Engine (GEE)	5 × 20 m	2014-2024: January - December
ERS 1/2 C-Band	VV	ESA Online Dissemination	12.5 × 12.5 m	1991 – 2000: October - March
Envisat C-Band	VV	ESA Online Dissemination	30 × 30 m	2002 – 2012: October - March
RADARSAT-1 C-Band	HH	Alaska Satellite Facility Distributed Active Archive Center	30 × 30 m	1995 – 2013: October - March
ALOS PALSAR L-Band	HH and HV	Alaska Satellite Facility Distributed Active Archive Center	10 × 10 m	2006 – 2011: October - March

While different platforms employ different naming conventions for processing levels, all datasets were Ground Range Detected (GRD). This means the products retained only the amplitude component of the raw signal, were multi-looked to reduce speckle noise, and were geometrically projected to ground range. Sentinel-1 and ALOS PALSAR data came with additional processing, including being calibrated to sigma^0 backscatter intensity and geometrically terrain-corrected. The other SAR sensor data came in a Level 1 format (no calibration to backscatter intensity and without geometric terrain correction), requiring further processing.

2.1.3 Ancillary Data

In addition to using Earth observation data to study these trends, there were several forms of ancillary data used to validate and supplement the Earth observations (Table 3). Partners from the USGS, Kalispel Tribe, and Selkirk Conservation Alliance provided in situ water temperature measurements. Additionally, the team acquired daily air temperature data from the Parameter-elevation Regressions on Independent Slopes Model (PRISM) for the Priest Lake region with a spatial resolution of 800 meters (See Appendix I for PRISM freezing dates from 1989 to 2024).

Table 3
Ancillary datasets used for validation and analysis

Ancillary Data	Time Period	Source
Priest River water temperature measurements	Summer 2018, Summer 2019	USGS in situ measurements
Upper Priest Lake monthly mean water surface temperature	2013-2024	USGS Landsat-8 ARD
Outlet bay and Priest River water temperature measurements	2011-2024	Kalispel Tribe
Priest Lake outlet water temperature	1993, 2017, 2021, 2023	Selkirk Conservation Alliance
Upper Priest Lake water temperature	1993, 1994, 2016, 2017, 2019, 2022, 2024	Selkirk Conservation Alliance
Air Temperature	1989-2024	PRISM

2.2 Data Processing

2.2.1 Multispectral Imagery

Optical imagery required various processing steps using Python v3.13.7 prior to analysis (Figure 2). For water surface temperature, the images were initially cropped to the region of interest to limit the amount of data that needed to be processed and then cloud masked. Pixel values from the thermal band of Landsat imagery were converted to degrees Celsius using Equation 1.

$$\text{Temp}=(\text{DN}\times 0.00341802) + 149.0 - 273.15 \quad (1)$$

where DN = digital numbers. The digital numbers are integer values assigned to each pixel in a digital image, are proportional to the units to which each band was estimated, and can be converted to a floating point version in those units using a linear transformation. The team masked data to three separate regions of interest: Main Priest Lake, Upper Priest Lake, and the Outlet Bay (the region surrounding the Outlet Dam). The team removed pixels that had values of less than -10°C as they were considered unrealistic and likely represented incomplete removal of cloud cover. Additionally, the team removed scenes that contained less than 25% of pixel coverage of the lake region of interest due to a lack of meaningful data (Figure 2).

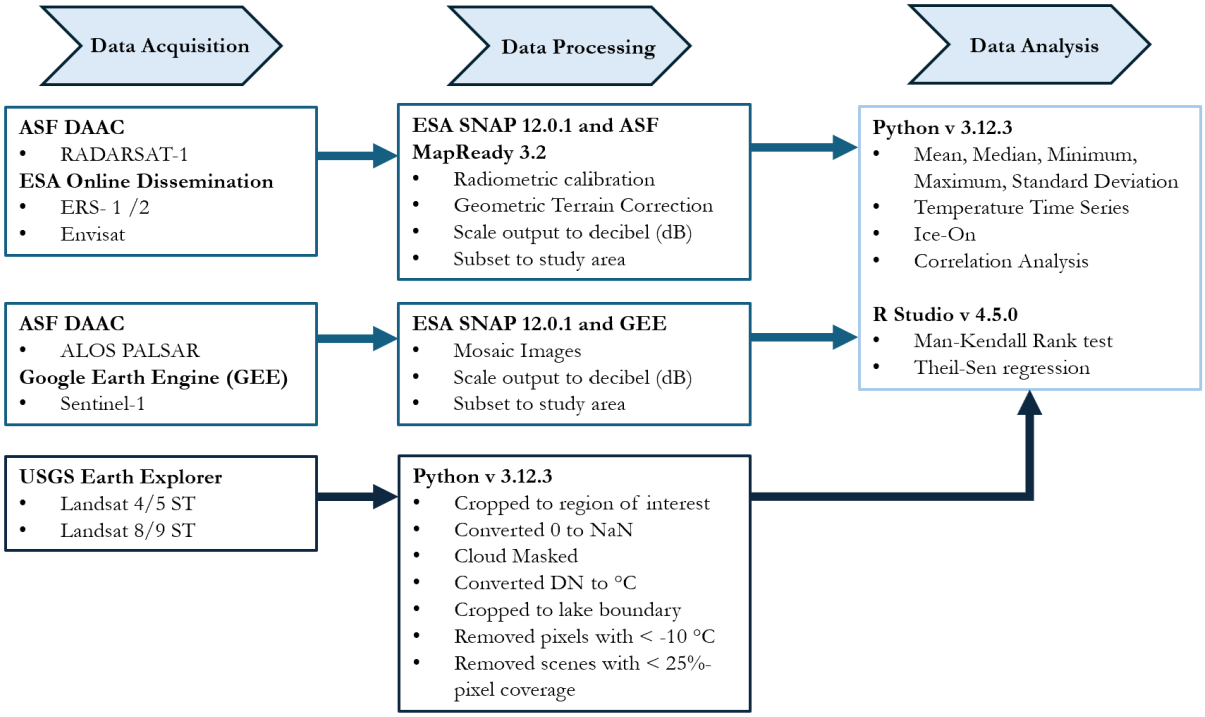

Figure 2. Workflow process for SAR imagery from data acquisition to analysis and for multispectral imagery from data acquisition to water temperature analysis.

The Landsat Collection 2 Level 1 optical bands were visually inspected for ice cover (panchromatic band when available and infrared when not). The team cropped images to the region of interest and then visually inspected for cloud coverage and removed from the data set if cloud coverage prevented reasonable interpretation. The team used Landsat Collection 2 Level 2 Surface reflectance product to evaluate ice extent from optical imagery. The team downloaded all available optical bands, cropped to the region of interest, and cloud masked. DN stored as pixel values in the optical bands required conversation to surface reflectance values using Equation 2:

$$\text{Surface Reflectance} = DN \times 0.0000275 - 0.2 \quad (2)$$

2.2.2 SAR Imagery

SAR data required several different implementations of processing due to the various data download platforms and file types. Sentinel-1 and ALOS PALSAR data came in processed formats that had already applied radiometric terrain calibration and geometric terrain correction (Figure 2). The team processed ERS 1 & 2 and Envisat data using the European Space Agency Sentinel Application Platform v12.0.1 (SNAP). RADARSAT-1 required the use of ASF (Alaska Satellite Facility) MapReady v3.2 to process the images due to the incompatibility of its Committee on Earth Observation Satellites (CEOS) format with SNAP. Within their respective software, the team processed imagery for radiometric calibration and geometric terrain correction. Prior to exporting to the GeoTIFF format, all the images had outputs converted to decibel (dB) scale to expand the data range and facilitate thresholding of water and ice surfaces. This was done because water typically exhibits low backscatter intensity on the linear scale. The team then used the processed data to extract the min, max, mean, median, and standard deviation for statistical analysis.

2.3 Data Analysis

2.3.1 Water Surface Temperature

The team analyzed processed Landsat thermal data based on region of interest: Priest Lake, Upper Priest Lake, and the Outlet Bay. For each processed Landsat image, the team calculated the mean, median,

maximum, and minimum temperature, along with the range and standard deviation. The team performed all data analysis in Python. The team compared mean water surface temperature values with in situ measurements and ancillary data (Table A1 and Figure A1) for validation.

2.3.2 Visual Ice Confirmation

The team analyzed optical images to determine if ice was present. Landsat 8 & 9 Panchromatic (Band 8) and Landsat 4 & 5 (Band 4) were used to visually inspect files dated November – May. The team removed scenes from the dataset with excessive cloud coverage to prevent ice misclassification. The team used a binary classification scheme to record the observations of ice-on Priest Lake (PL) and Upper Priest Lake (UPL) (Table 4) from the visual inspection of Landsat imagery. The classification scheme is progressive, such that a scene with full ice coverage of Priest Lake would have 1 in all classification columns.

Table 4

Ice coverage classification system for visually inspected optical imagery

Classification	Explanation
Ice	0 = no ice observed 1 = ice presence observed
Partial UPL	0 = no ice observed on upper priest lake 1 = some ice observed on upper priest lake
UPL ice	0 = upper priest lake is not fully covered by ice 1 = upper priest lake appears fully covered by ice
Partial PL	0 = no ice observed on main priest lake 1 = some ice observed on partial priest lake
Full coverage	0 = main priest lake is not fully covered by ice 1 = the majority of priest lake appears ice covered

2.3.3 Ice Detection

SAR imagery was mainly used for detecting ice presence on Priest Lake and Upper Priest Lake. Ice presence was initially determined based on a thresholding metric of the mean backscatter, which varied based on sensor and polarization (Table 5). Sentinel-1 data had a dense temporal resolution that overlapped with optical observations, making it feasible to systematically threshold ice and water pixels values specific to the study area for each polarization. Threshold values for ice/water pixels in Sentinel-1 images were determined by analyzing Gaussian distribution of backscatter values (Appendix B). Small, homogeneous polygons were selected from co-registered SAR and optical images acquired on the same date or within a day's interval, where surface conditions were clearly identifiable as either ice (full and thin) or water. The overlap between ice and water samples was more pronounced in the VH (cross-polarized) backscatter than in the VV (co-polarized) backscatter, indicating lower contrast between ice and water in VH (Figure B1). Thus, the team selected VV backscatter from Sentinel-1 for ice analysis.

Ice threshold values for the other satellites were derived from the work of Nghiem & Leshkevich (2007), who conducted a comprehensive analysis of ice threshold values specific to these platforms across the Great Lakes region. This range of decibel values allowed for a threshold to be applied to the mean decibel values obtained. From this, a simple binary system was used to detect ice, where if the threshold condition was met a 1 was assigned to that date and if it was not met a 0 was assigned to that date.

Table 5
Threshold values for the mean decibel SAR readings across various platforms and polarizations

Platform	Polarization	Mean Decibel (dB) Threshold
RADARSAT-1	HH	-4.0 ≥$\overline{dB}$ ≥ -25.0
ERS-1 & 2	VV	
Envisat	VV	
ALOS PALSAR	HH and HV	
Sentinel-1	VV	-10.0≥$\overline{dB}$≥-22.0
Sentinel-1	VH	-18.0≥$\overline{dB}$≥-35.0

To improve the detection of ice presence from SAR imagery, a classification system requiring three of four conditions must be met. The team used ice presence as a condition in Upper Priest Lake, a smaller, shallower, lake which has less hydro-motion, meaning it is more likely to freeze before Priest Lake. Since ice formation requires water surface temperatures below 0°C, the team used water surface temperature derived from Landsat as another condition. On bodies of water the size of Priest Lake, there needs to be at least seven days consecutive days of freezing air temperatures for ice formation to occur (Culpepper et al., 2024). Thus, the team utilized a Negative Degree Day (NDD) Index as an additional condition. Lastly, the team checked optical image ice confirmation: a comparison inspection of ice to the SAR imagery within a week of acquisition. Using these conditions, the team developed a schematic for SAR detected ice presence based on three of these four conditionals being met.

2.3.4 Assessment of Ice Extent

The team assessed ice extent by calculating the percent of the lake area covered by ice-on dates when earth observation imagery was accessible. Due to the sparse nature of available earth observations in the pre-Sentinel era, the team limited assessment of ice extent from 2014-2024. Three different differencing indices were generated from the optical bands to help classify ice presence: the Normalized Difference Infrared Index (NDII), the Normalized Difference Snow Index (NDSI), and the Normalized Difference Water Index (NDWI), in addition to a simple thresholding of the saturation level of the green band (Table 6). This method follows the work of Sojka et al. (2023), where thresholds of multiple indices were used alongside the threshold of a single optical band to classify lake ice.

The team determined specific thresholding values for identifying ice-on Priest Lake (Table 6) by evaluating Landsat scenes where visual confirmation of ice presence was clear (e.g. Figure 3) and applied to all available Landsat scenes. Using any one of the four thresholds alone did not appear to classify ice as well as using a combined thresholding classification scheme from all four parameters. The team classified open water with a single threshold value using NDWI > 0.5.

Table 6.
Threshold values used from optical bands to classify ice presence from available Landsat imagery, using the green, Near Infrared (NIR), and the Short-Wave Infrared 1 (SWIR1) bands

Differencing Index	Equation	Lake Ice Classification Threshold	Open Water Classification Threshold
Green band	Green band	Green > 0.2	
NDII	(NIR – SWIR1) / (NIR+ SWIR1)	NDII > 0.5	
NDSI	(GREEN – SWIR1) / (GREEN + SWIR1)	NDSI > 0.8	
NDWI	(GREEN – NIR) / (GREEN + NIR)	NDWI > 0.0	NDWI > 0.5

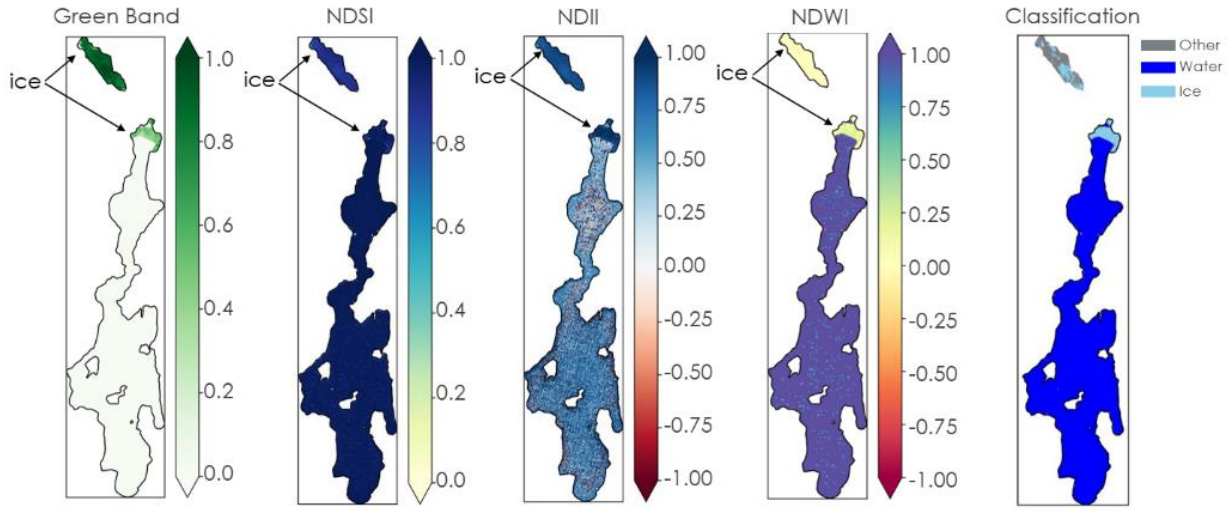

Figure 3. Landsat scene from March 6, 2024 masked to Upper Priest Lake and Priest Lake showing the surface reflectance of the green band, NDSI, NDII, NDWI, and classified scene.

In addition to the optical data, the team used Sentinel-1 SAR data to estimate ice extent for the same period (2014 – 2024) to assess temporal changes in ice extent. To maintain consistency with the spatial resolution of the optical data in counting the total number of pixels, the team resampled Sentinel-1 imagery to a 30 meter resolution prior to analysis. The team derived ice extent as the proportion of pixels that satisfied the VV threshold of ice (Table 5).

2.3.5 Assessment of Temporal Trend in Air and Water Surface Temperature

The team determined long-term trends in water surface temperature by fitting a simple linear regression to the mean water surface temperature of each region of interest. The team analyzed seasonal and monthly trends in temperature data using a Mann-Kendall rank test to detect significant increase or decrease in trends, and Theil-Sen regression was employed to evaluate the magnitude of change in temperature over time (Vicente-Serrano et al., 2025). For Theil-Sen regression, higher slope values indicate a rapid increase in temperature over time. Both Mann-Kendall and Theil-Sen regression are nonparametric statistical models which do not rely on any assumptions of statistical probability assumptions, thus offering robustness against outliers in observed temperature values. For seasonal trends, the team defined winter as December, January, and February; spring as March, April, and May; summer as June, July, August, and September; and fall as October and November.

2.3.6 Assessment of Temporal Trends in Ice Phenology

To determine ice phenology on Priest Lake, the team defined ice-on date as the first day ice was detected in the SAR time series, while ice-off (the final day ice was observed) was too ambiguous to be effectively determined. The team analyzed long-term trends in ice-onset using simple linear regression applied to annual ice-on dates. The team expressed ice-on dates as the number of days elapsed since October 1st. Due to limited SAR imagery before Sentinel-1, ice-on dates were unavailable for some winter seasons, particularly between 1998 and 2005; consequently, the team excluded these years from the analysis.

Within an ice season (i.e., the period within a year where ice typically forms, November – March), observations of ice presence oscillated between detected ice presence and ice-free conditions. Based on variability in detected presence of ice within a single season, the team wanted to understand 1) how ice presence for each month has changed over the study period, and 2) the regime shifts in monthly ice phenology. To assess monthly changes in the presence of ice during the study period, the team fitted a generalized linear model (GLM) with binomial error distribution and logit link function using R version 4.5.0. The team set the response variable as ice presence (yes/no), and the predictor variables as fixed effect of

"Year" and "Month", and their interaction effect of "Year" and "Month". More details about the statistical models and analysis are in Appendix C.

2.3.7 Correlation Analysis between Ice Phenology and Lake Surface Temperature

To evaluate the association between summer lake surface temperature and ice-on timing, the team performed a linear regression analysis. The team defined summer lake surface temperature as the annual maximum observed between June and September. The team assessed model fit and statistical significance using the coefficient of determination (R^2) and p-value respectively.

2.3.8 Correlation Analysis between Air Temperature Variables and Ice Phenology

Given the sporadic detection of ice presence within the ice season, the team assessed temperature variability to gain a better understanding of these conditions on Priest Lake. However, the team found a lack of temporal resolution for water surface temperature to assess weekly temperature effect on ice presence. Thus, the team used air temperature instead. To assess the effect of air temperature on presence of ice in each month during the study period, the team used a classification model using eXtreme Gradient Boosting (XGBoost; Chen & Guestrin 2016). More details about model formulations and analysis are in Appendix D.

3. Results

3.1 Analysis of Results

3.1.1 Trends in Air and Water Surface Temperature

Linear regression analyses of the mean derived water surface temperature show an increase over the study period (Figure 4). Priest Lake showed an increase of 0.05°C per year, Upper Priest Lake showed an increase of 0.10°C per year, and the Outlet Bay showed an increase of 0.06°C per year.

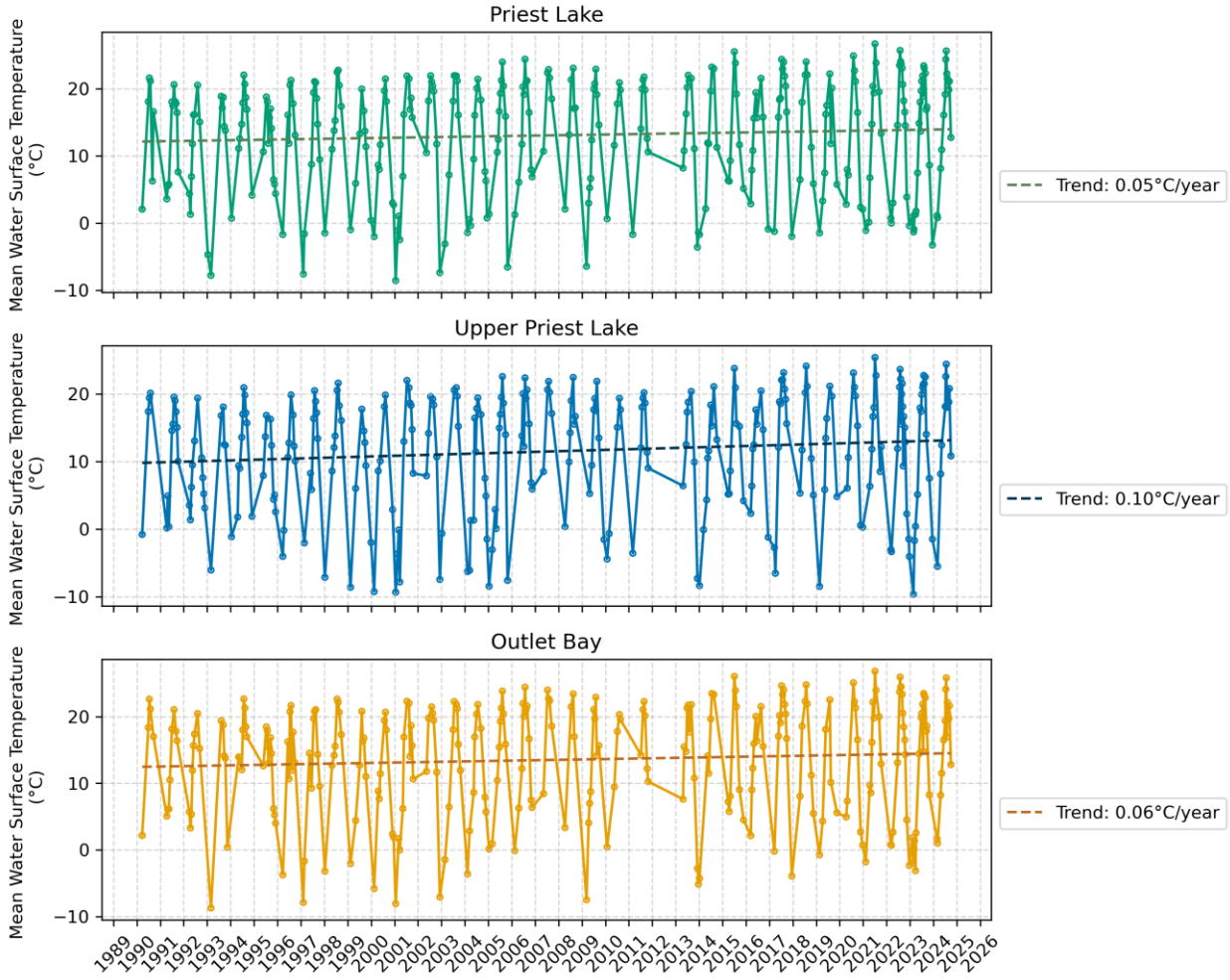

Figure 4. Long-term trends in mean water surface temperature on Priest Lake, Upper Priest Lake, and the Outlet Bay.

Over the study period, the team observed significant trends in the summer season for air temperature and water surface temperature on both lakes (Figure 5A, Table E1). A monthly analysis of air temperature and water surface temperature allowed for more comprehensive results (Figure 5B, Table E2). Air temperature showed a significant increase in January, March, May, July, and August. The air temperature had a significant decrease in February and April. Water surface temperature in Upper Priest Lake showed significant increases during several months: April, May, June, July, August, and September. Water surface temperature in Priest Lake showed significant increases in May, June, August, and September with significant decreases in November and December. Results on maximum and minimum temperature trends are presented in Appendix E (Figures E1-E3).

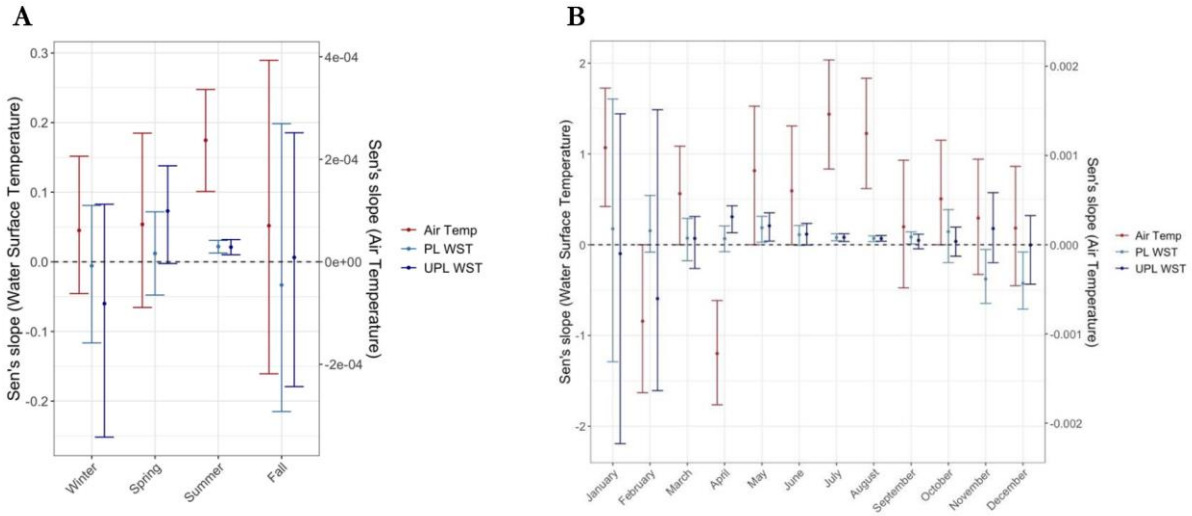

Figure 5. Seasonal (A) and monthly (B) trend in mean air temperature (right axis) and water surface temperature at Priest Lake and Upper Priest Lake (left axis) across the study period.

3.1.2 Assessment of Trends in Ice Phenology

3.1.2.1 Observed ice presence on Priest Lake

Assessment of trends in ice phenology from 1990-2024 is limited by available earth observations of ice presence (Figure 6). During the first two decades of the study period (1990–2010), SAR imagery indicated ice-onset mostly occurred in November; however no optically verified imagery showed any ice formation during the month of November in any year of this study. The latter portion of the study period (2012–2024) showed a gradual shift toward later ice-onset dates, often in December or January. Ice typically persisted from January through March across most years. Ice-off timing was challenging to estimate due to limited data: pre-Sentinel-1 (2014-2024) was not evaluated past March 30, which contributes to the earlier appearance of ice-off trends in the first 24 years of this study. Available optical and SAR imagery indicate ice persists on Priest Lake in March and April most years, but no earth observations indicate ice presence during the month of May. Similar trends are evident on Upper Priest Lake (Appendix F).

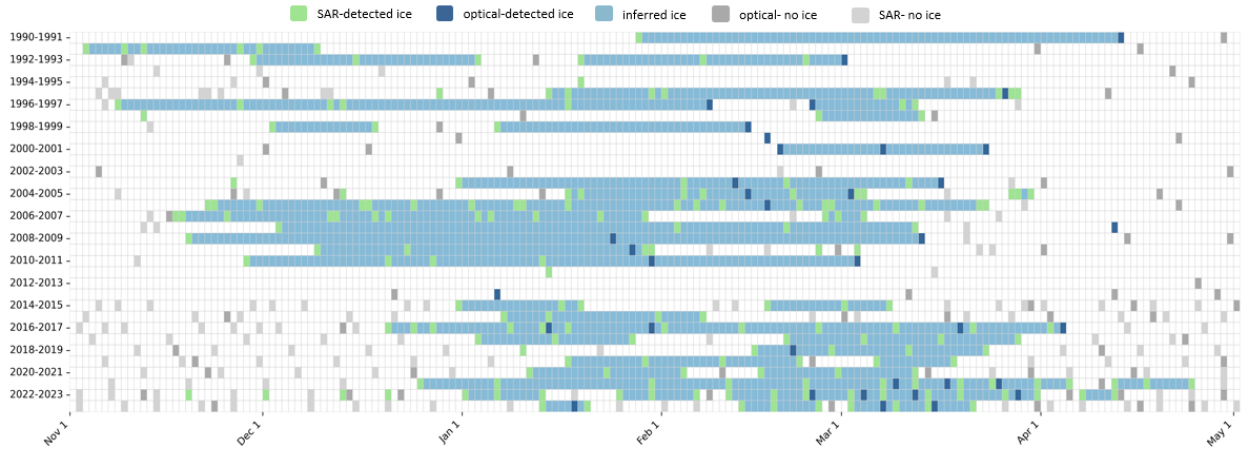

Figure 6. Observations of ice presence on Priest Lake determined by SAR imagery (green) and optical imagery (navy blue), along with observations of ice-free conditions as determined by SAR imagery (light grey) and optical data (dark grey). Inferred ice presence (light blue) is used to show the inference of ice presence persisting between one earth-observation of ice presence and the next.

3.1.2.2 Assessment of trends in ice-on phenology

Available Earth observations revealed an apparent shift to later onset of ice over the study period (Figure 7), with estimated annual shifts of approximately 1.4 days at Priest Lake and 1.2 days at Upper Priest Lake. With this understanding of recent delay in ice-on, the team conducted further analysis to understand how the observed delay in ice-on may change the presence of ice for each month during the ice season over the study period. In general, the team found a significant decline in the occurrence of ice presence across the entire ice season over the study period at both Priest Lake and Upper Priest Lake. At Priest Lake, the annual probability of observing ice declined by 1% in November and 12 % in December and increased by 2.5% in March (Appendix C, Figure C1A). At Upper Priest Lake, annual probability of observing an ice declined by 10% in November and 8 % in December and increased by 6% in March (Appendix C, Figure C1B).

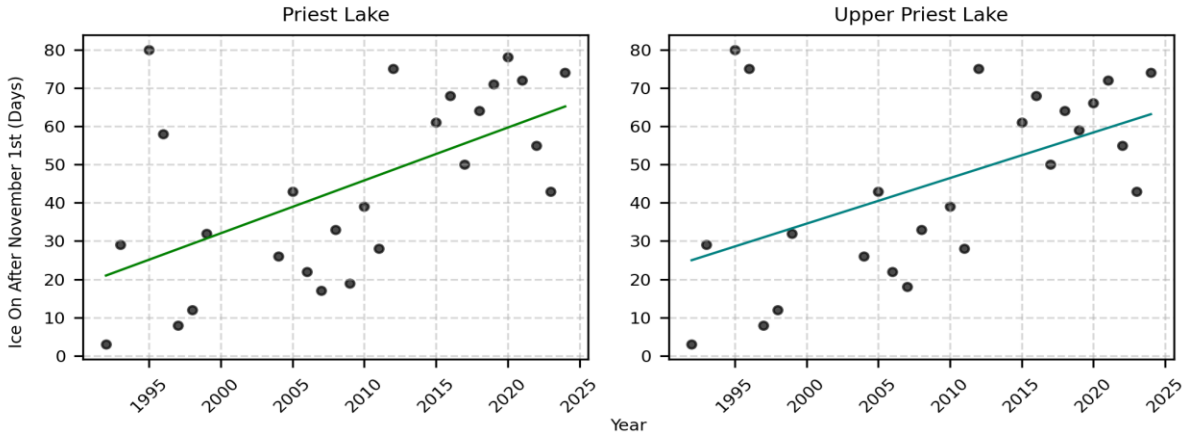

Figure 7. Trend in ice-on timing for Priest Lake ($R^2 = 0.34$, p-value < 0.01, slope = 1.4) and Upper Priest Lake ($R^2 = 0.27$, p-value < 0.01, slope = 1.2).

3.1.2.3 Assessment of regime shift in ice presence over the study period

If ice-on is delayed, a higher frequency of ice presence in later months of the ice season is expected compared to earlier months in recent years. The team defined early ice presence as ice detected prior to December 31st of every year, while late ice presence as ice detected after December 31st. The team found a significant decline in the probability of presence of ice earlier in the season at both study sites (Estimate±SE = -0.08±0.02, z-value=-4.2, p<0.01). 25% and 22% of the ice presence occurred prior to January of the winter season at Priest Lake and Upper Priest Lake, respectively. At Priest Lake, 31% of the early ice formation occurred in the first ten years of the study period (1990-1999), while only 18% of the early ice formation occurred in last ten years of the study period (2014-2024; Appendix C, Figure C2A). At Upper Priest Lake, there was 11% more of early ice presence in the first ten years of the study period compared to the last ten years of the study period (Appendix C, Figure C2B), indicating that ice presence is mostly delayed at both sites, especially in recent years. Similarly, at Priest Lake there was 37% less late ice presence in the first ten years of the study period compared to the last ten years of the study period. There was about 41% less late ice presence on Upper Priest Lake in the first ten years of the study period compared to the last ten years of the study period, indicating a potential phenological shift in frequency of detected ice presence towards later in the ice season (Appendix C).

3.1.3 Evaluation of temporal changes in ice extent

Calculated ice extent from classified optical data is limited to 19 data points on Priest Lake and 24 data points on Upper Priest Lake between 2014-2024 due to limited cloud-free optical imagery with sufficient pixel coverage of each lake basin. For example, ice extent calculations from available optical imagery show greater ice coverage of Priest Lake in March 2017 compared to March 2022 (Figure G1); however, the limited number of data prohibits a robust analysis of temporal trends in ice coverage and extent over this study

period. The results of percent lake ice cover are impacted by cloud coverage, which appears as "no data" in the classification scheme and does not contribute to the percent of pixels classified as ice, even when conditions suggest that ice coverage is highly likely beneath the cloud-affected regions. Therefore, percent ice coverage calculated from optical imagery should be interpreted with caution.

A timeseries of lake ice coverage by season using both Landsat and SAR imagery (Figure 8) shows that generally, Upper Priest Lake has a greater percentage of ice coverage than Priest Lake, as expected. Optically derived values of percent ice coverage generally agree with those calculated from SAR data. Discrepancies between optical and SAR data where optical imagery shows less ice coverage than SAR data could be explained by cloud-impacted optical imagery. Significant ice coverage appears to exist during the months of January, February, and March for all years between 2014-2024. Sparse data during the ice formation and ice melting seasons (assumed November-December and May, respectively), prevent effective assessment of temporal trends of ice extent.

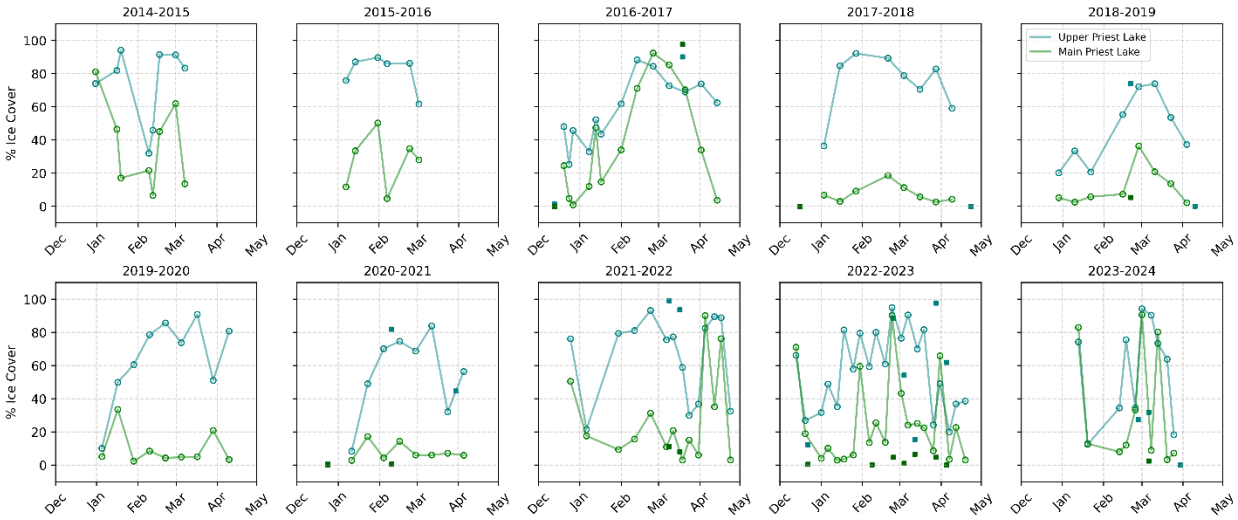

Figure 8. Ice extent of Upper Priest Lake (teal) and Priest Lake (green) shown as percent of lake area covered by ice as detected by Landsat optical imagery (squares) and SAR data (circles).

3.1.3 Correlation Analysis

3.1.3.1 Correlation between Water Surface Temperature and Ice-on

Maximum summer (June–September) water surface temperature exhibited a moderate positive association with ice onset for Priest Lake ($R = 0.54$, $p < 0.01$) and Upper Priest Lake ($R = 0.50$, $p < 0.01$) (Figure 9). However, the low R^2 values (Priest Lake=0.29; Upper Priest Lake=0.25) underscores a weak explanatory power. This indicates that summer surface temperature alone accounts for a limited proportion of the variability in ice-on timing.

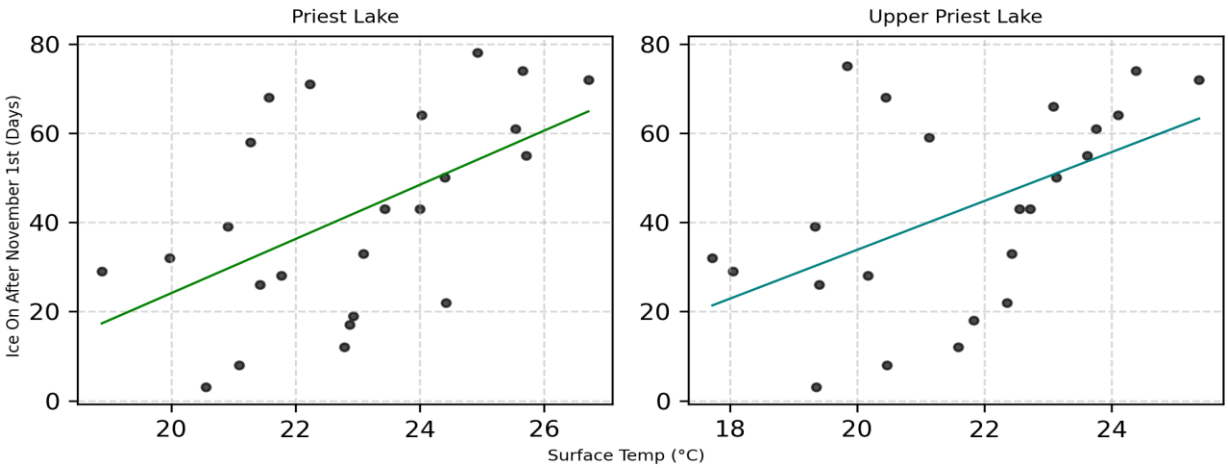

Figure 9. Correlation between maximum summer water surface temperature and ice-on for Priest Lake and Upper Priest Lake.

3.1.3.2 Correlation between Air Temperature Variables and Ice presence

At both sites, mean air temperature four weeks prior to detecting ice contributed strongly to the probability of ice presence (Figure D1). The probability of predicting ice presence decline significantly as the mean air temperature four weeks prior to the ice-on increases above 0°C (Figure D2, D3). More detail information about the result of this analysis is in Appendix D.

3.2 Errors & Uncertainties

There is significant uncertainty in the results for both assessing trends in water surface temperature and lake ice phenology due to limited data. In the analysis of water surface temperature, there were only 316 days of our 34-year (12,783 day) study period where the team was able to extract water surface temperature values from Priest Lake using Landsat imagery. More water surface temperature measurements were available during summer months, due to higher cloud coverage in winter months, which may skew the results from our long-term trend analysis toward higher values. Further, the exclusion of pixel values <-10°C during data processing could have skewed derived water surface temperature values towards higher results. Analysis of changing water surface temperatures by month and season were similarly limited by sparse data (Appendix H, Table H1). Since the data points are not evenly distributed temporally, the results may be skewed in ways that do not reflect true trends. Maximum water surface temperatures used for correlation analyses were the highest observed values from Landsat data, but the dates of available data varied year to year; therefore, the maximum water surface temperature may not be truly representative (Figure A3)

Uncertainty in ice-on dates stems from two key limitations: 1) challenges in correctly determining ice presence from SAR imagery, and 2) difficulty in accurately capturing the ice-on date from sparse data. Accurately detecting ice presence from SAR imagery is limited by the ability to appropriately characterize backscatter thresholds needed to classify ice-on Priest Lake, combined with the challenge of differentiating between wind and ice. Another signature confusion challenge arises from the overlap between ice and open water, particularly during the presence of thin ice. Even with VV backscatter, distinguishing these conditions can be problematic (Figure B1). Finally, detections of ice presence on Priest Lake (Figure 7) reveal a discrepancy between optically verified and SAR-derived ice conditions in some years. This discrepancy caused uncertainty to carry over into further analysis, such that nearly half (48%) of the data used in the ice-on timing trend analysis and its correlation with water surface temperature have at least 15 days of uncertainty in the ice-on calculation, which contributes to substantial uncertainty in assessing changes in ice phenology over the course of this study period.

4. Conclusions

4.1 Interpretation of Results

This project employed remote sensing techniques to help the ICL, USGS, and other local stakeholders to understand trends in ice-phenology, water surface temperature, and their relationship for Priest Lake and Upper Priest Lake over the past three decades. Thermal imagery provides longer-term water surface temperature measurements of Priest Lake, Upper Priest Lake, and the Outlet Bay than is available from in situ measurements. Water surface temperature data derived from the Landsat constellation appears to be increasing, indicating that Priest Lake may be changing similarly with other lakes around the world (Korver er al., 2024). Continuing increase in water surface temperatures could impact the lake ecology of Priest Lake and the broader Priest River watershed (Mejia et al., 2021). Earth observations indicated ice may be present on Priest Lake between October 31 – May 1. Studies to assess changes in ice phenology should cover this period to effectively evaluate changes in ice duration and extent. Seasonal trends in ice presence on Priest Lake and Upper Priest Lake are difficult to accurately assess with Earth observations alone due to limited data, particularly in the pre-Sentinel-1 era. With these limitations in mind, the team observed a delay in ice-on on Priest Lake and Upper Priest Lake over the course of the study period, aligning with global trends (Basu et al., 2024). Warming water surface temperatures may be contributing to a change in ice phenology; however, there is a minimal correlation between observed maximum water surface temperature and ice-on date in this study. To more fully assess the relationship between warming waters and changing ice conditions, more frequent and reliable measurements are needed. The results from this feasibility study provide the partners with long-term data that can be used in conjunction with in situ measurements to make informed decisions in their advocacy for watershed management strategies at Priest Lake.

4.2 Feasibility & Partner Implementation

The use of remote sensing to analyze long-term trends in water surface temperature and ice phenology is manageable but has several limitations. Multispectral imagery can be used to effectively expand observations of water surface temperature beyond available in situ measurements (e.g. Figure A2, A3, A4). However, Landsat-derived temperature data are severely limited in the winter months due to persistent cloud coverage. Optical imagery experiences similar challenges when observing ice: cloud coverage blocks viewing of ice presence, severely limiting available observations to ~70 dates of ice observations across a 34-year period. When looking at SAR imagery for detecting ice presence, even more challenges arise. SAR data prior to Sentinel-1 (2014) are relatively limited, making it challenging to determine the first and last days where ice has been present. Additionally, the use of SAR data for detecting ice is heavily impacted by wind disturbances affecting the surface roughness which may result in false positives identifying ice from water. This poses a challenge for classifying the presence of ice. It is recommended that additional data sets be used for this classification. This includes air temperature data, daily wind data, and involving the community with local observations. Though remote sensing has its limitations, there are meaningful ways to move forward with it. To start, the study period should be expanded to include all months in which there is a possibility of ice (November – May), allowing for proper evaluation of ice trends. In evaluating ice presence, optical data from Sentinel-2 could validate ice coverage during the Sentinel era. Denser concentrations of multispectral data and SAR data could improve the ability to assess prior years, while future Landsat launches may provide more data with higher resolution. The use of remote sensing and Earth observations is feasible, however high attention to detail, supplemental data sets, and an expanding study period are required. In order to effectively determine long term trends and the relationship between water surface temperature and ice presence on Priest Lake, Earth observations can be informative when used in conjunction with other data sets.

5. Acknowledgements

- Jennifer Ekstrom, North Idaho Director of the Idaho Conservation League
- Dr. Francine Mejia, Biologist, USGS Forest and Rangeland Ecosystem Science Center
- Eric Bernsten, Fisheries Biologist, Kalispel Tribe of Indians, Natural Resources Department
- Amy Anderson, Executive Director, Selkirk Conservation Alliance (SCA)
- Ephraim Romesberg, Citizen Science Project Water Quality Lead Technician, SCA
- Benjamin Holt and Manu Tom, Jet Propulsion Laboratory (JPL)
- Dr. Kenton Ross, NASA Langley Research Center
- Gwenyth Greco, NASA DEVELOP Lead (California – JPL)
- Brent Bowler, NASA DEVELOP Project Coordination Fellow (Virginia – Langley)

This material contains modified Copernicus Sentinel data (2014-2024), processed by ESA.

Any opinions, findings, and conclusions or recommendations expressed in this material are those of the author(s) and do not necessarily reflect the views of the National Aeronautics and Space Administration.

This material is based upon work supported by NASA through contract 80LARC23FA024.

6. Glossary

Earth observations – Satellites and sensors that collect information about the Earth's physical, chemical, and biological systems over space and time
Ice duration – How long the ice was on the water from its formation to melting
Ice extent – The amount of lake ice present, quantified by the percent of total lake area with ice-on it.
Ice-off – The last date that ice was seen on the water
Ice-on – The first date that ice was seen on the water
Ice phenology – the study of the timing of ice formation (ice-on) and ice break-up (ice-off).
Ice presence – Anytime that ice has been detected on a body of water
Ice season – Period within the year when ice is likely to form (usually between November to March)
PL – Priest Lake
SAR – Synthetic aperture radar
UPL – Upper Priest Lake

7. References

Basu, A., Culpepper, J., Blagrave, K., & Sharma, S. (2024). Phenological shifts in lake ice cover across the Northern Hemisphere: A glimpse into the past, present, and the future of lake ice phenology. *Water Resources Research, 60*(9), e2023WR036392. https://doi.org/10.1029/2023WR036392

Breiman, L. (2001). Random forests. *Machine Learning, 45*(1), 5-32. https://doi.org/10.1023/A:1010933404324

Calvin, K., Dasgupta, D., Krinner, G., Mukherji, A., Thorne, P. W., Trisos, C., Romero, J., Aldunce, P., Barrett, K., Blanco, G., Cheung, W. W. L., Connors, S., Denton, F., Diongue-Niang, A., Dodman, D., Garschagen, M., Geden, O., Hayward, B., Jones, C., … Péan, C. (2023). *IPCC, 2023: Climate Change 2023: Synthesis Report. Contribution of Working Groups I, II and III to the Sixth Assessment Report of the* Intergovernmental *Panel on Climate Change [Core Writing Team, H. Lee and J. Romero (eds.)]. IPCC, Geneva, Switzerland.* Intergovernmental Panel on Climate Change (IPCC). https://doi.org/10.59327/IPCC/AR6-9789291691647

Chen, T., & Guestrin, C. (2016). Xgboost: A scalable tree boosting system. In KDD '16: Proceedings of the 22nd ACM SIGKDD International Conference on Knowledge Discovery and Data Mining (pp. 785-794). https://doi.org/10.1145/2939672.2939785

Culpepper, J., Huang, L., Woolway, R. I., & Sharma, S. (2024). Widespread loss of safe lake ice access in response to a warming climate. *PLOS ONE*, *19*(12), e0313994. https://doi.org/10.1371/journal.pone.0313994

Culpepper, J., Sharma, S., Gunn, G., Magee, M. R., Meyer, M. F., Anderson, E. J., Arp, C., Cooley, S. W., Dolan, W., Dugan, H. A., Duguay, C. R., Jones, B. M., Kirillin, G., Ladwig, R., Leppäranta, M., Long, D., Magnuson, J. J., Pavelsky, T., Piccolroaz, S., … Yang, X. (2025). One-Hundred fundamental, open questions to integrate methodological approaches in lake ice research. *Water Resources Research*, *61*(5), e2024WR039042. https://doi.org/10.1029/2024WR039042

Earth Resources Observation and Science (EROS) Center. (2020). Landsat 8-9 Operational Land Imager / Thermal Infrared Sensor Level-2, Collection 2 [dataset]. U.S. Geological Survey. https://doi.org/10.5066/P9OGBGM6

Earth Resources Observation and Science (EROS) Center. (2020). Landsat 4-5 Thematic Mapper Level-2, Collection 2 [dataset]. U.S. Geological Survey. https://doi.org/10.5066/P9IAXOVV

Earth Resources Observation and Science (EROS) Center. (2020). Landsat 8-9 Operational Land Imager / Thermal Infrared Sensor Level-1, Collection 2 [dataset]. U.S. Geological Survey. https://doi.org/10.5066/P975CC9B

Earth Resources Observation and Science (EROS) Center. (2020). Landsat 4-5 Thematic Mapper Level-1, Collection 2 [dataset]. U.S. Geological Survey. https://doi.org/10.5066/P918ROHC

Korver, M. C., Lehner, B., Cardille, J. A., & Carrea, L. (2024). Surface water temperature observations and ice phenology estimations for 1.4 million lakes globally. *Remote Sensing of Environment*, *308*, https://doi.org/10.1016/j.rse.2024.114164

Leppäranta, M., & Wen, L. (2022). Ice phenology in Eurasian lakes over spatial location and altitude. *Water, 14*(7), 1037. https://doi.org/10.3390/w14071037

Lin, Y., Lindenschmidt, K. E., Lü, H., Zhu, Y., Liu, M., Chen, T., & Xu, Y. (2025). Modeling climate change effects on river ice thickness in the Northern Hemisphere. *Journal of Hydrology, 660*, 133268. https://doi.org/10.1016/j.jhydrol.2025.133268

Mejia, F. H., Connor, J. M., Kaufmann, P. R., Torgersen, C. E., Berntsen, E. K., & Andersen, T. K. (2021). Integrating regional and local monitoring data and assessment tools to evaluate habitat conditions and inform river restoration. *Ecological Indicators*, *131*, 108213. https://doi.org/10.1016/j.ecolind.2021.108213

Murfitt, J., & Duguay, C. R. (2020). Assessing the performance of methods for monitoring ice phenology of the world's largest high arctic lake using high-density time series analysis of Sentinel-1 data. *Remote Sensing*, *12*(3). https://doi.org/10.3390/rs12030382

Nghiem, S. V., & Leshkevich, G. A. (2007). Satellite SAR remote sensing of Great Lakes ice cover, Part 1. Ice backscatter signatures at C band. *Journal of Great Lakes Research*, *33*(4), 722–735. https://doi.org/10.3394/0380-1330(2007)33[722:SSRSOG]2.0.CO;2

O'Reilly, C. M., Sharma, S., Gray, D. K., Hampton, S. E., Read, J. S., Rowley, R. J., Schneider, P., Lenters, J. D., McIntyre, P. B., Kraemer, B. M., Weyhenmeyer, G. A., Straile, D., Dong, B., Adrian, R., Allan, M. G., Anneville, O., Arvola, L., Austin, J., Bailey, J. L., … Zhang, G. (2015). Rapid and highly variable warming of lake surface waters around the globe. *Geophysical Research Letters*, *42*(24), 10,773-10,781. https://doi.org/10.1002/2015GL066235

PRISM Group, Oregon State University *Air Temperature* [Data set]. Retrieved July, 2025 from https://prism.oregonstate.edu

Piccolroaz, S., Zhu, S., Ladwig, R., Carrea, L., Oliver, S., Piotrowski, A. P., Ptak, M., Shinohara, R., Sojka, M., Woolway, R. I., & Zhu, D. Z. (2024). Lake water temperature modeling in an era of climate change: data sources, models, and future prospects. *Reviews of Geophysics*, *62*(1), e2023RG000816. https://doi.org/10.1029/2023RG000816

Shaposhnikova, M., Duguay, C., & Roy-Léveillée, P. (2023). Bedfast and floating-ice dynamics of thermokarst lakes using a temporal deep-learning mapping approach: Case study of the Old Crow Flats, Yukon, Canada. *The Cryosphere*, *17*(4), 1697-1721. https://doi.org/10.5194/tc-17-1697-2023

Sharma, S., Richardson, D. C., Woolway, R. I., Imrit, M. A., Bouffard, D., Blagrave, K., Daly, J., Filazzola, A., Granin, N., Korhonen, J., Magnuson, J., Marszelewski, W., Matsuzaki, S.-I. S., Perry, W., Robertson, D. M., Rudstam, L. G., Weyhenmeyer, G. A., & Yao, H. (2021). Loss of ice cover, shifting phenology, and more extreme events in northern hemisphere lakes. *Journal of Geophysical Research: Biogeosciences*, *126*(10), e2021JG006348. https://doi.org/10.1029/2021JG006348

Sojka, M., Ptak, M., & Zhu, S. (2023). Use of Landsat satellite images in the assessment of the variability in ice cover on polish lakes. *Remote Sensing*, *15*(12), 3030. https://doi.org/10.3390/rs15123030

Vicente-Serrano, S.M., Tramblay, Y., Reig, F. et al. (2025). High temporal variability not trend dominates Mediterranean precipitation. *Nature,* 639, 658–666. https://doi.org/10.1038/s41586-024-08576-6

Xu, L., Feiner, Z. S., Frater, P., Hansen, G. J. A., Ladwig, R., Paukert, C. P., Verhoeven, M., Wszola, L., & Jensen, O. P. (2024). Asymmetric impacts of climate change on thermal habitat suitability for inland lake fishes. *Nature Communications*, *15*(1), 10273. https://doi.org/10.1038/s41467-024-54533-2

8. Appendices

Appendix A: *Water Surface Temperature Validation*

Water surface temperature measurements derived from Landsat thermal bands were validated by comparing with in situ measurements from the Selkirk Conservation Alliance, the Kalispel Tribe, and the USGS Water Temperature of Lakes in the Conterminous U.S. Using the Landsat 8 Analysis Ready Dataset Raster Images from 2013-2024 (USGS Landsat8 ARD).

Table A1

Ancillary water surface temperature datasets. SCA measurement sites locations are shown in Figure A2

Region	Selkirk Conservation Alliance	Kalispel Tribe	USGS
Upper Priest Lake	UPLK (Upper Priest Lake)		Landsat8 ARD
Priest Lake	MOSQ (Mosquito Bay) BREK (Beaver Creek) SQUA (Squaw Bay) HUCK (Huckleberry Bay) PLNO (North of Huckleberry Bay) DIST (Distillery Bay) GNAR (near Granite Creek Marina) KALI (Kalispell Bay) PLSO (Priest Lake South) CAV Bay (Cavanaugh Bay) COOL (Coolin Bay)		
Outlet Bay	OUTL (Outlet Bay) LWPR (Lower Priest River)	OUTL	

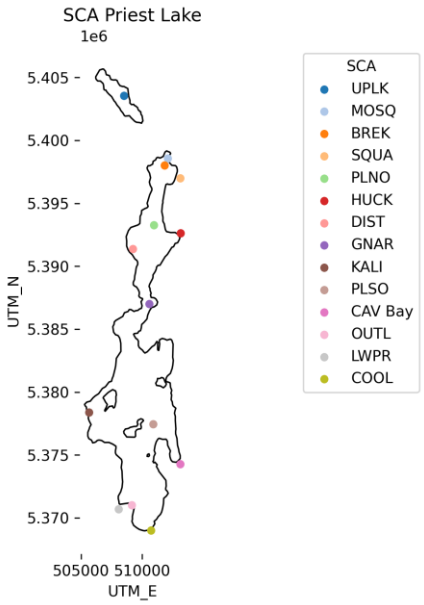

Figure A1. Water temperature measurement sites used by the Selkirk Conservation Alliance Citizen Science Water Quality Monitoring Program.

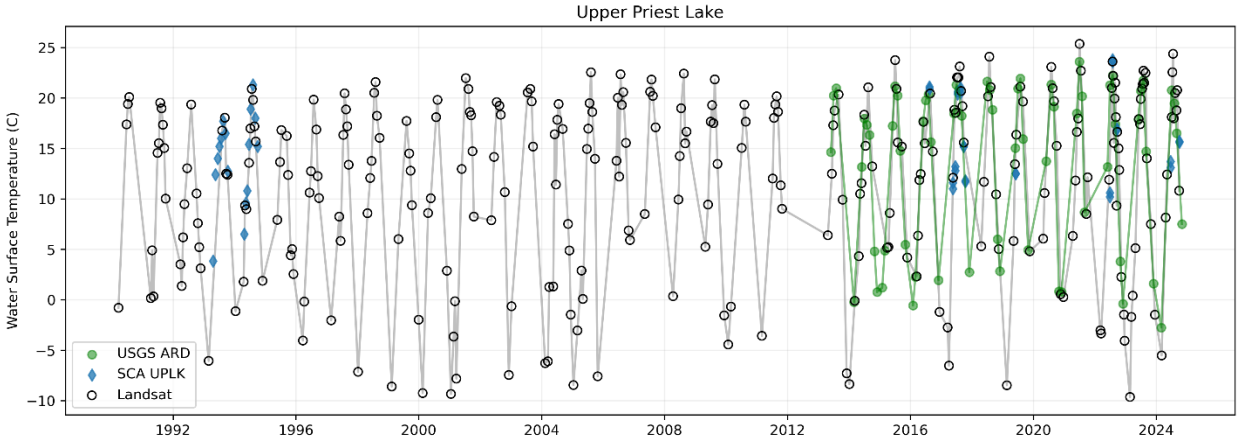

Figure A2. Water surface temperature from Upper Priest Lake taken from the mean temperature from each processed Landsat scene (black), in situ values taken by the Selkirk Conservation Alliance (blue) at depths <1.5m below the surface, and mean values extracted from the USGS Landsat 8 ARD dataset (green).

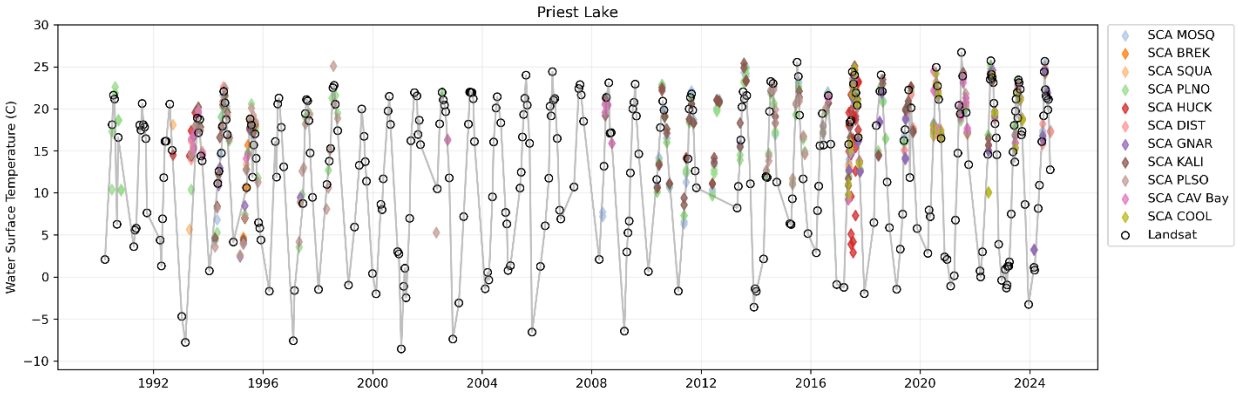

Figure A3. Water surface temperature from Priest Lake taken from the mean temperature from each processed Landsat scene (black) alongside in situ values taken by the Selkirk Conservation Alliance (colored by site) at depths <1.5m below the surface.

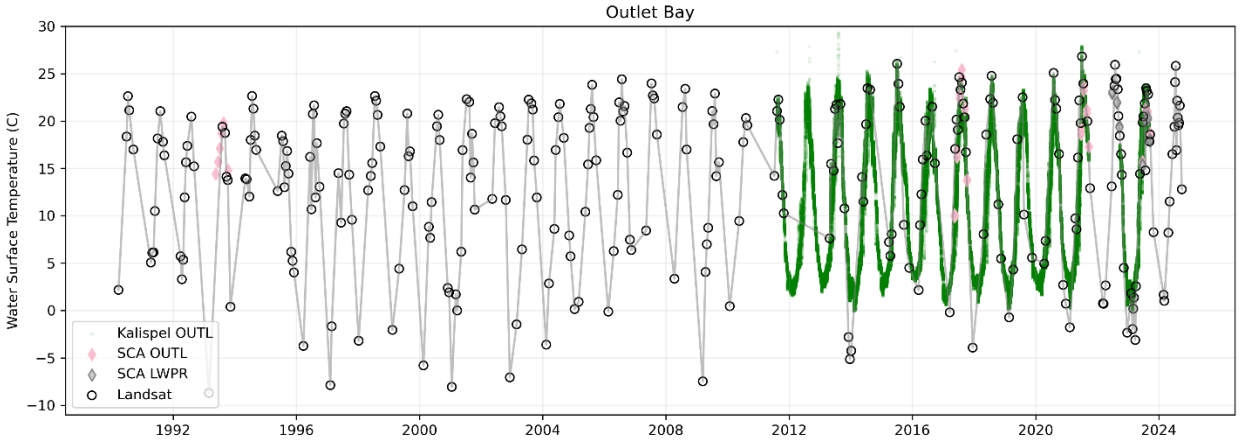

Figure A4. Water surface temperature from the Outlet Bay, showing the mean temperature of the region from each processed Landsat scene (black), in situ values collected by the Selkirk Conservation Alliance at the Outlet Bay and Lower Priest River (colored by site) at depths <1.5m below the surface, and in situ values from the Outlet area taken by the Kalispel Tribe (green).

Appendix B. *SAR Backscatter Thresholds for Sentinel-1*

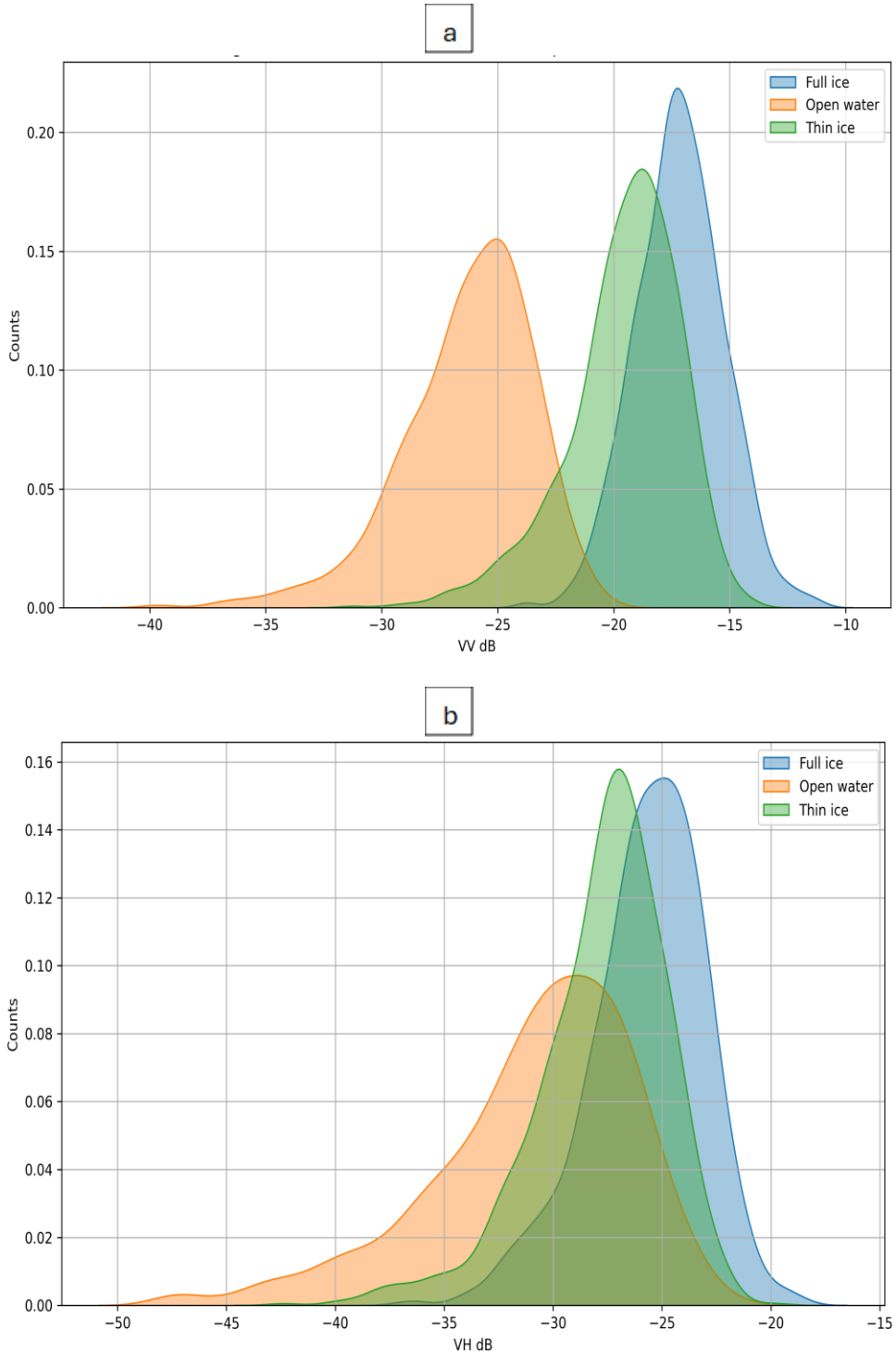

Figure B1. Distribution of water, thin and full ice samples for VV (a) and VH (b) backscatter

Appendix C: *Assessment of Trends in Lake Ice Presence*

Within an ice season (i.e., the period within a year where ice typically forms, November – March), we observed that ice comes on and off multiple times. For instance, we can detect ice in early December and not late December but rather detect ice in January or in February. We do not know the cause of this sporadic occurrence in ice; perhaps variability in temperature can cause ice to form and melt multiple times within the ice season. Based on variability in presence of ice within a single season, we were interested in understanding how ice presence for each month within the ice season has changed over the study period. Thus, in this study we defined ice presence as whether we detected ice in each month during the ice season. To assess monthly changes in the presence of ice during the study period, we fitted a generalized linear model (GLM) with binomial error distribution and logit link function ("glm" function in R ver 4.5.0). The response variable was a Bernoulli variable of ice presence (yes=1) and ice absence (no=0) for each month. The predictor variables were fixed effect of "Year" and "Month" (during the ice period; November, December, January, February, and March), and interaction effect of "Year" and "Month". The fixed effect of "Year" assessed the overall annual trend in probability of ice being presence over the study period, while the fixed effect of "Month" assessed the relative differences in presence of ice between months. The interaction effect of "Year" and "Month" estimated how the probability of being detected for a particular has changed over the study period. The full model parameterization is as described in equation (3) below:

$$E(y)= \beta_0+\beta_1 Year+ \beta_2 Month+ \beta_3 Month*Year+e\ldots \quad (3)$$

Where $E(y)$ = estimated probability of monthly ice presence β_0, β_1, β_2 , and β_3 are the intercept and effect size for Year, Month, and Year*Month interaction, and e is the residual error. We also assessed regime shift in ice phenology (Basu et al. 2024). To do this, we converted monthly ice-on dates to the day of the year relative to December 31st. December 31st was the baseline date and thus was set to day zero (Basu et al., 2024). We then calculated anomaly for presence of ice in each month as number of days prior to day zero that we observed the presence of ice in a particular and the number of days after day zero. The number of days prior to day zero got negative anomaly days values while the number of days after December 31st got positive anomaly values. For instance, the presence of ice-on November 23 was -38 days, while presence of ice-on February 3rd was +34 days. We then defined any ice-on dates prior to day zero as "early ice presence" and ice formation dates after day zero as "late ice presence".

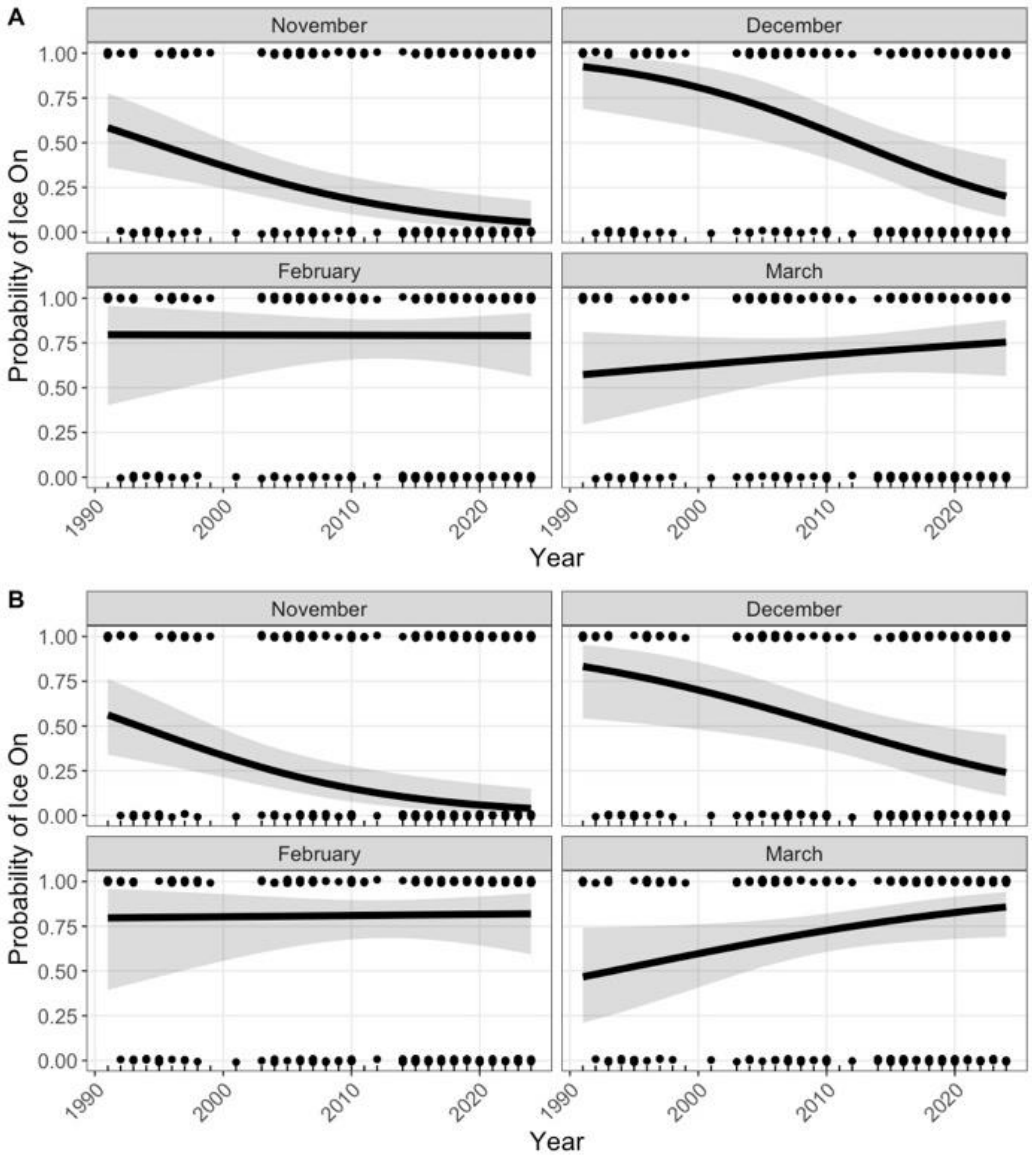

Figure C1. Trend in monthly probability of observing ice at (A) Priest Lake and (B) Upper Priest Lake over the study period. We do not show a plot for January because ice was present on the lakes for almost every observation in January throughout the study period. The results indicate that the probability of observing ice is delayed in recent years, with a decrease in ice presence. in November and December months, but an increased probability of ice presence after December.

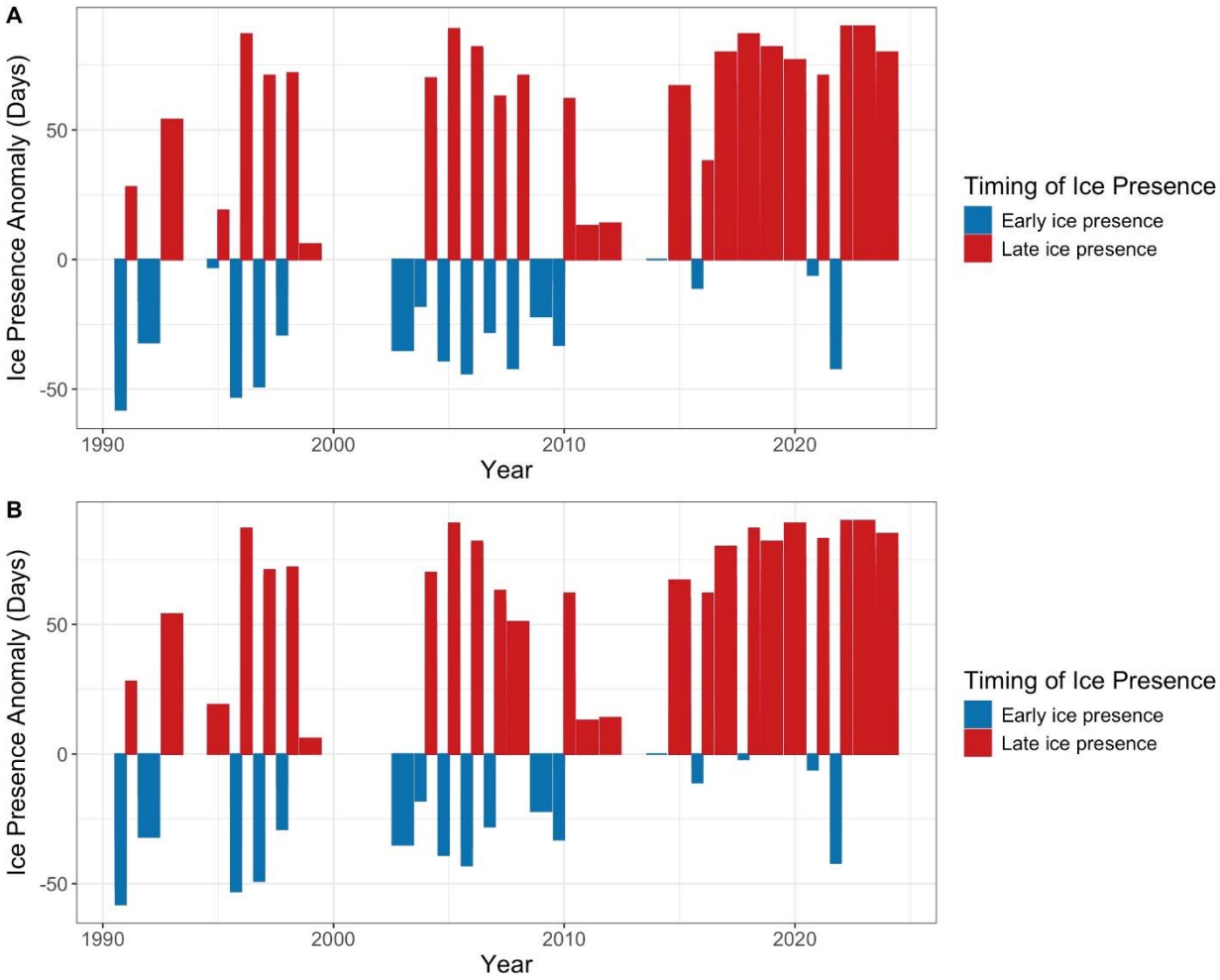

Figure C2. Phenological shift in ice presence at (A) Priest Lake and (B) Upper Priest Lake over the study period. Blue bars indicate that ice formation occurred earlier (i.e., prior to January 1st; negative y-axis values) and red bars indicate that ice formation occurred late or was delayed (i.e., occurred after January 1st; positive y-axis values).

Appendix D: *Correlation Analysis between Air Temperature Variables and Ice Phenology*

Given the sporadic detection of ice presence within the ice season, we were interested in understanding whether temperature variability may explain the observed pattern. However, we lacked the temporal resolution for water surface temperature to assess weekly temperature effect on ice presence. Thus, we used air temperature instead.

To assess the effect of air temperature on presence of ice in each month during the study period, we fitted a classification model using two machine learning algorithms: Random Forest (Breiman et al. 2001) and eXtreme Gradient Boosting (XGBoost; Chen and Guestrin 2016). We fitted both models in R. For Random Forest we used the "randomForest" package, and "xgboost" package for XGBoost. The response variable was a binary variable of whether there was ice was presence or not within each month during ice season. We used 20 different predictor variables which directly and indirectly relate to air temperature. The direct air temperature variables were weekly mean, minimum, and maximum air temperature and their time-lags ranging from one week to four weeks prior to monthly ice formation. The purpose of this was to account for the delay effect of air temperature on monthly ice formation (Leppäranta et al., 2022; Lin et al., 2025). The indirect air temperature variables were a cumulative number of freezing days in the past one to four weeks prior to ice formation. Prior to fitting the models, we divided the data sets into training (1991-2018) and testing (2019-2024) data sets. We fitted the model to the training dataset and validated it using the testing dataset. We evaluated the performance of both XGBoost and the Random Forest model using area under curve (AUC). The XGBoost model had the highest AUC value (0.71) compared to the Random Forest model (AUC=0.25). Thus, we focused on the XGBoost model as the preferred model for our analysis. We assessed the contribution of each variable to the prediction of ice presence by plotting the feature importance calculated from the XGBoost model. We also calculated the SHAPLEY values, which quantifies the log-odds of predicting ice presence for each predictor variable, from the XGBoost model using the "SHAPforxgboost" package in R.

At both sites, mean air temperature four weeks prior to detecting ice contributed strongly to the probability of ice presence (Append D, Figure D1). The probability of predicting ice presence decline significantly as the mean air temperature four weeks prior to the ice-on increases above 0°C (Append D, Figure D2&3). This also implies that, ice formed earlier is likely to melt if mean air temperarure in the past four weeks gets warmer. This findings explains the observed sporadic pattern in presence in Figure 7. The second most important variables was minimum air temperature three weeks prior to ice-on (Append D, Figure D1). Increased in minimum air temperature three weeks prior to ice-on significantly declined the probability of predicting ice-on at Priest Lake (Append D, Figure D2&3). The third most important variables were maximum temperature (at PL) and minimum temperature (UPL) three weeks prior to ice-on. Increased maximum air temperature three weeks prior to ice-on significantly declined the probability of observing the presence of ice at Upper Priest Lake. Increased minimum air temperature four weeks prior to ice-on significantly declined the probability of observing ice presence at Upper Priest Lake. Similary, the probability of ice presence declined significantly with increasing mean temperature (Append D, Figure D2&3). The rest of the variables contributed less than 1% to the prediction of ice-on (Append D, Figure D1 A&B).

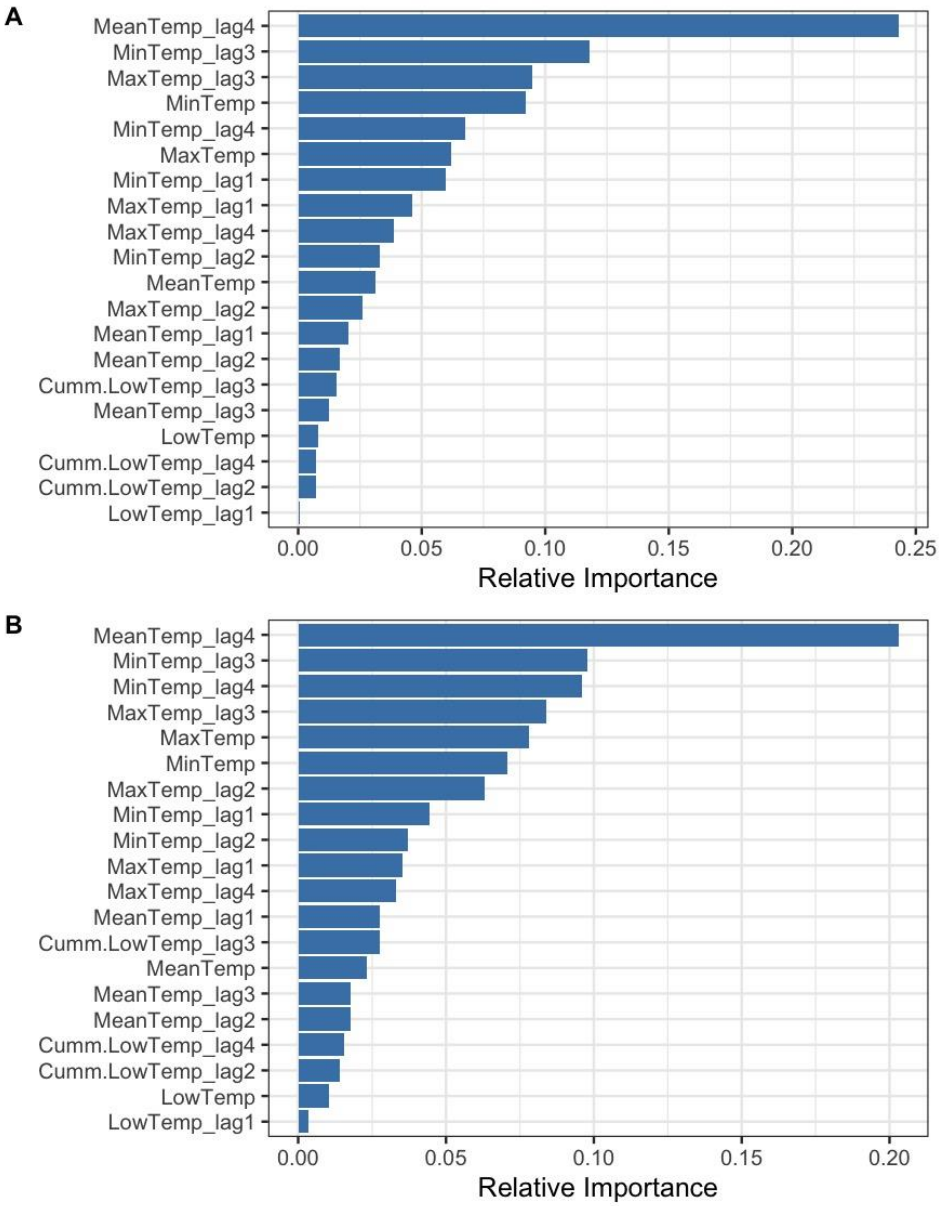

Figure D1. Relative variable importance predicting the probability of ice presence over the study period at (A) Priest Lake and (B) Upper Priest Lake. Large relative importance value (ranked from largest variable to the least) indicate variables with the greatest contribution to predicting ice presence.

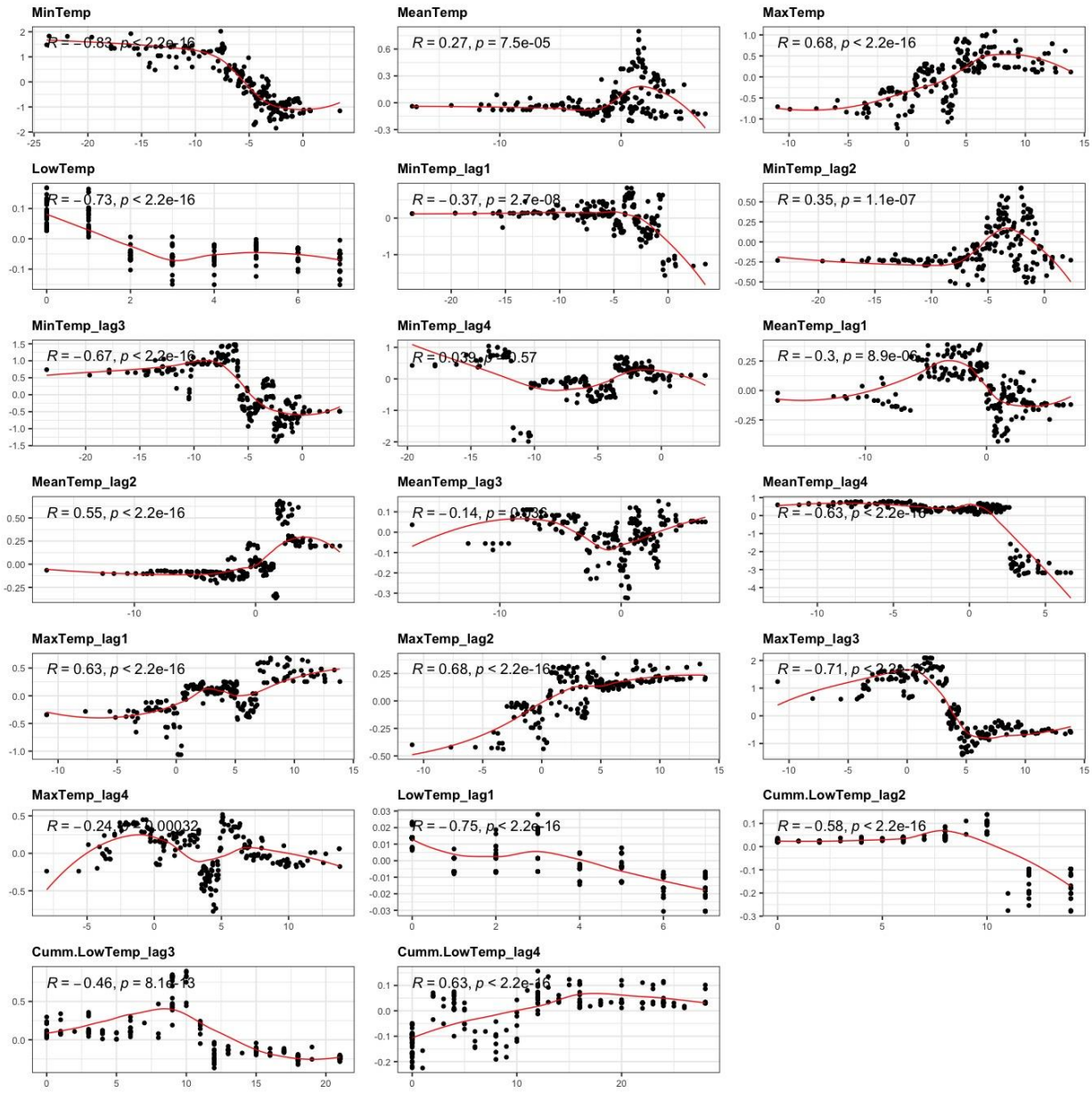

Figure D2. SHAP log-odd contribution of different temperature variable to the probability of ice-on at Priest Lake. The y-axis depicts the log-odd contribution: positive values mean increase the log-odds of predicting ice-on; and negative values means decrease the log-odds of predicting ice-on. The x-axis shows the values of the predictor variable. The predictor variable is labelled on top of each panel. The SHAP log-odd contribution was derived from the XGBoost model.

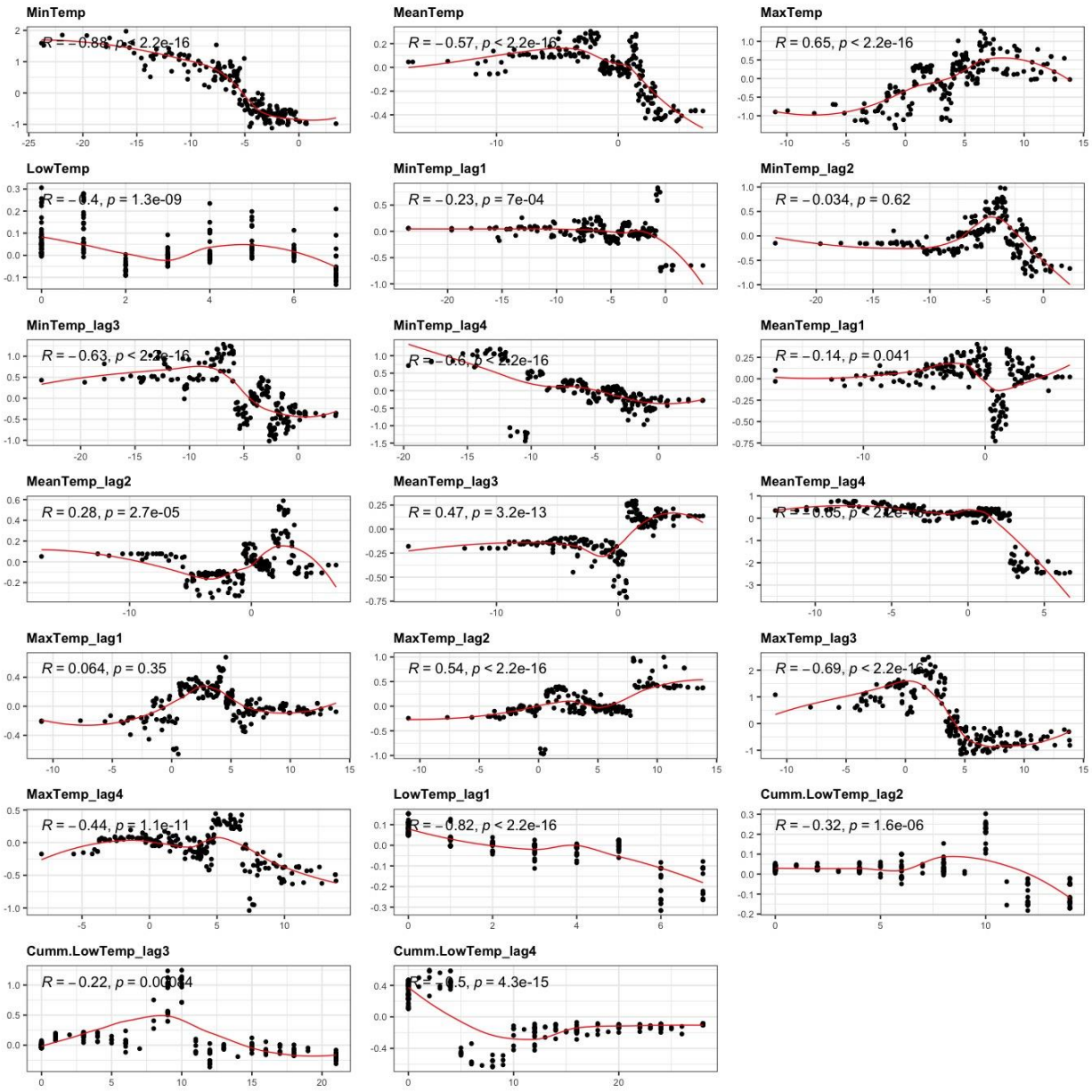

Figure D3. SHAP log-odd contribution of different temperature variable to the probability of ice-on at Upper Priest Lake. The y-axis depicts the log-odd contribution: positive values mean increase the log-odds of predicting ice-on; and negative values means decrease the log-odds of predicting ice-on. The x-axis shows the values of the predictor variable. The predictor variable is labelled on top of each panel. The SHAP log-odd contribution was derived from the XGBoost model.

Appendix E: *Seasonal and Monthly Trends in Air and Water Surface Temperature*

The Sen's slope estimates the magnitude of rate of change in temperature per year. Each value on the y-axis (estimated as Sen's slope) indicates the annual rates of change in temperature (°C) during the study period. The dots are the mean Sen's slope values, and the error bars represent the 95% confident interval (CI). Cases when the CI are completely above the black horizontal dashed lines indicate significant increase in temperature, while cases when the CI are completely below indicates significant decrease in temperature.

Table E1.
Seasonal trends in mean water surface temperature and air temperature with significant results (p <0.05) bolded and in colored by temperature type.

	Priest Lake Water			Upper Priest Lake Water			Air Temperature		
Season	**Sen's Slope**	**Mann-Kendall Tau**	**p**	**Sen's Slope**	**Mann-Kendall Tau**	**p**	**Sen's Slope**	**Mann-Kendall Tau**	**p**
Winter	-0.006	-0.01	0.95	-0.06	-0.11	0.33		0.01	0.33
Spring	0.01	0.04	0.66	0.08	0.18	0.02		0.01	0.33
Summer	**0.02**	**0.23**	**<0.01**	**0.02**	**0.21**	**<0.01**	**0.0002**	**0.05**	**<0.01**
Fall	-0.03	-0.03	0.8	0.05	0.07	0.5		0.008	0.59

Table E2.
Monthly trends in mean water surface temperature and air temperature with significant results (p <0.05) bolded and colored by temperature type.

	Priest Lake Water			Upper Priest Lake Water			Air Temperature		
Season	**Sen's Slope**	**Mann-Kendall Tau**	**p**	**Sen's Slope**	**Mann-Kendall Tau**	**p**	**Sen's Slope**	**Mann-Kendall Tau**	**p**
January	0.18	0.07	0.90	-0.10	0	1	**0.001**	**0.07**	**<0.01**
February	0.15	0.25	0.23	-0.60	-0.21	0.54	**-0.0009**	**-0.04**	**0.03**
March	0.07	0.14	0.42	0.05	0.06	0.73	**0.0006**	**0.04**	**0.03**
April	0.06	0.12	0.41	**0.30**	**0.44**	**<0.01**	**-0.001**	**-0.08**	**<0.01**
May	**0.18**	**0.31**	**0.01**	**0.24**	**0.41**	**<0.01**	**0.0008**	**0.05**	**0.02**
June	0.11	0.21	0.09	**0.15**	**0.30**	**0.02**	0.0006	0.03	0.10
July	**0.08**	**0.35**	**<0.01**	**0.09**	**0.30**	**<0.01**	**0.001**	**0.09**	**<0.01**
August	**0.069**	**0.38**	**<0.01**	**0.06**	**0.27**	**<0.01**	**0.001**	**0.08**	**<0.01**
September	**0.09**	**0.22**	**0.04**	0.03	0.07	0.53	0.0002	0.01	0.54
October	0.14	0.14	0.42	0.11	0.15	0.34	0.0005	0.03	0.11
November	**-0.38**	**-0.56**	**0.03**	-0.12	-0.27	0.24	0.0003	0.02	0.35
December	**-0.43**	**-0.41**	**0.05**	-0.26	-0.18	0.43	0.0002	0.01	0.53

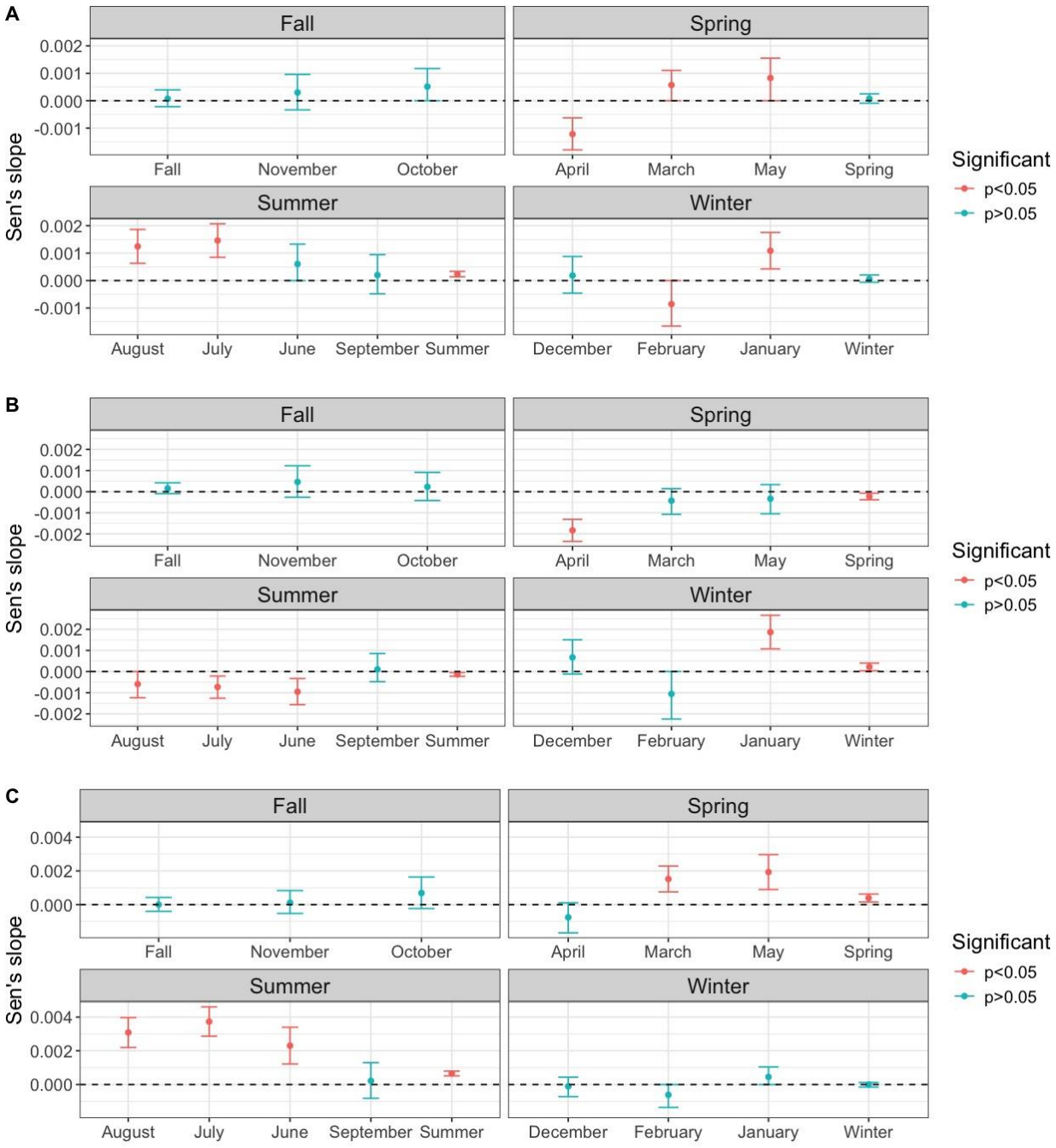

Figure E1. Seasonal and monthly trends in (A) mean, (B) minimum, and (C) maximum annual air temperature over the study period. The Sen's slope (y-axis) measures the magnitude of rate of increase or decrease in trend. A significant increase or decrease in trend was assessed by the Mann-Kendall Rank test.

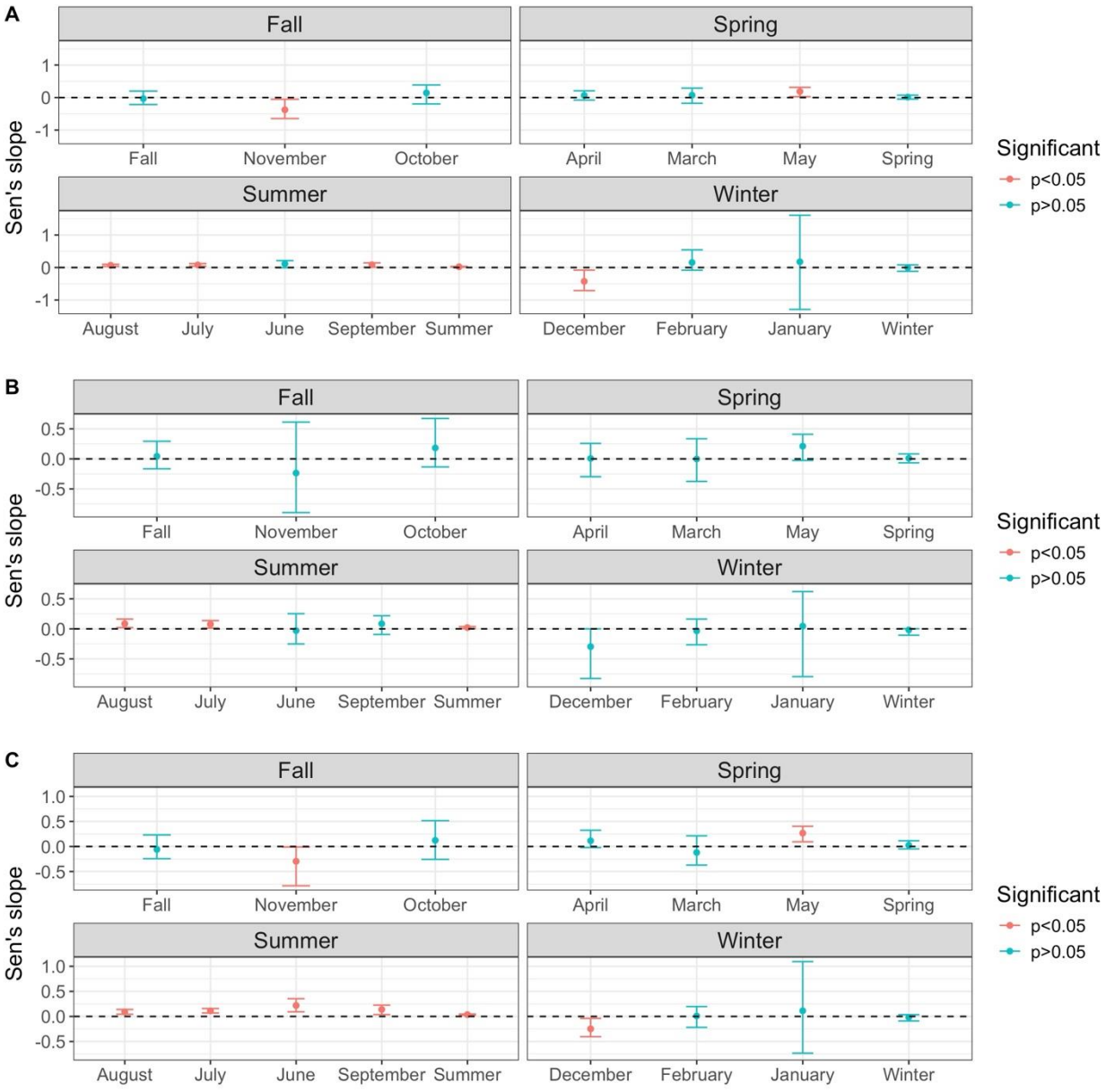

Figure E2. Seasonal and monthly trend at Priest Lake in (A) mean, (B) minimum, and (C) maximum annual water surface temperature over the study period. The Sen's slope (y-axis) measures the magnitude of rate of increase or decrease in trend. A significant increase or decrease in trend was assessed by the Mann-Kendall Rank test.

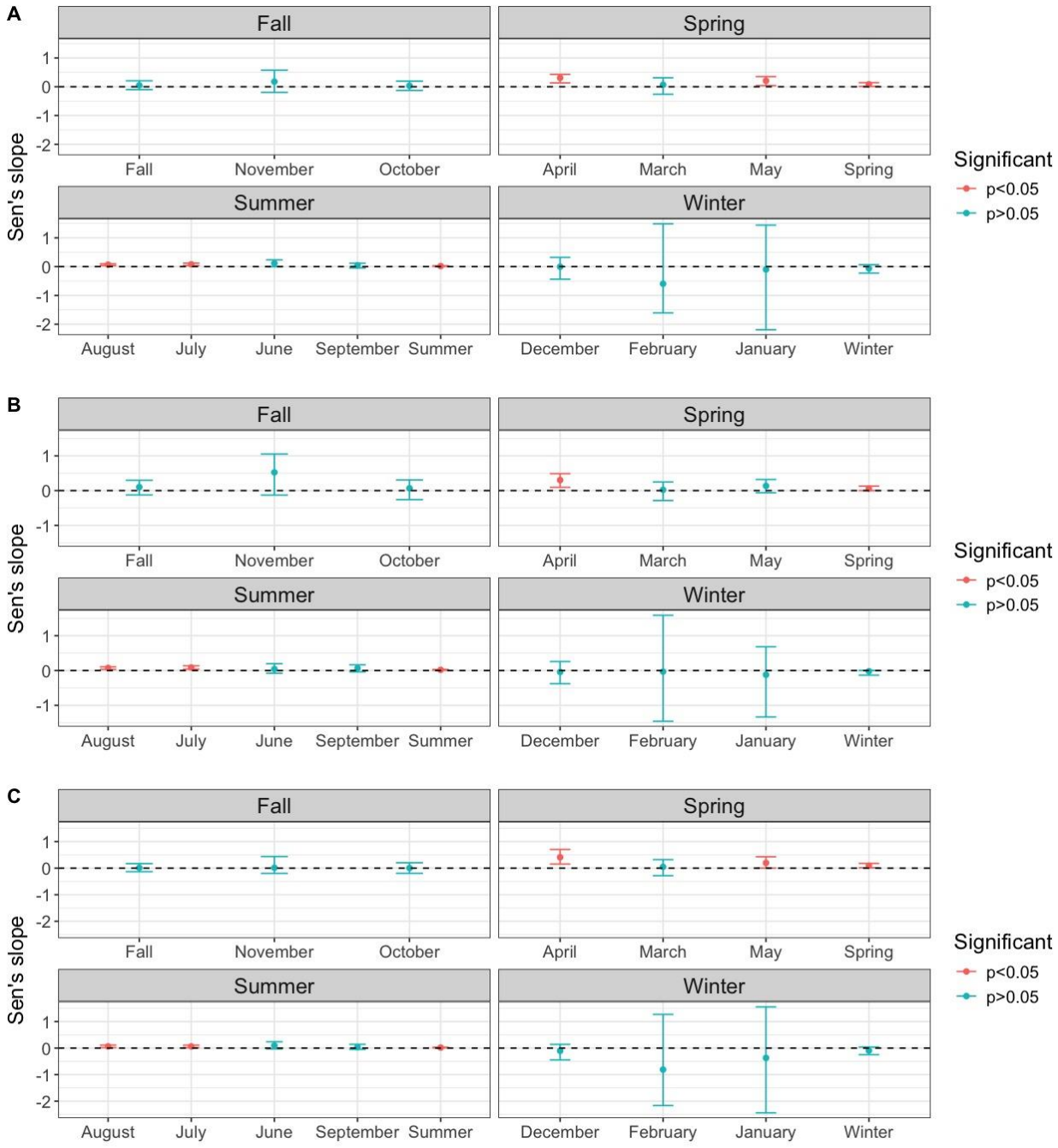

Figure E3. Seasonal and monthly trend in Upper Priest Lake (A) mean, (B) minimum, and (C) maximum annual water surface temperature over the study period. The Sen's slope (y-axis) measures the magnitude of rate of increase or decrease in trend. A significant increase or decrease in trend was assessed by the Mann-Kendall Rank test.

Appendix F. *Detected Ice Presence on Upper Priest Lake*

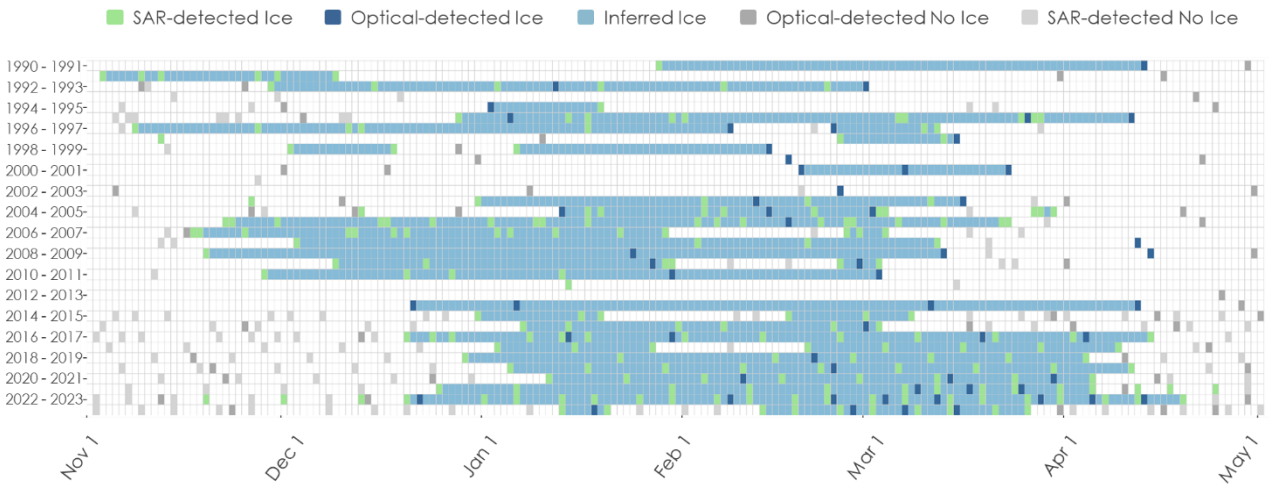

Figure F1. Observations of ice presence on Upper Priest Lake determined by SAR imagery (green) and optical imagery (navy blue), along with observations of ice-free conditions as determined by SAR imagery (light grey) and optical data (dark grey). Inferred ice presence (light blue) is used to show the inference of ice presence persisting between one earth-observation of ice presence and the next.

Appendix G. *Ice coverage extent calculated from classified Landsat data*

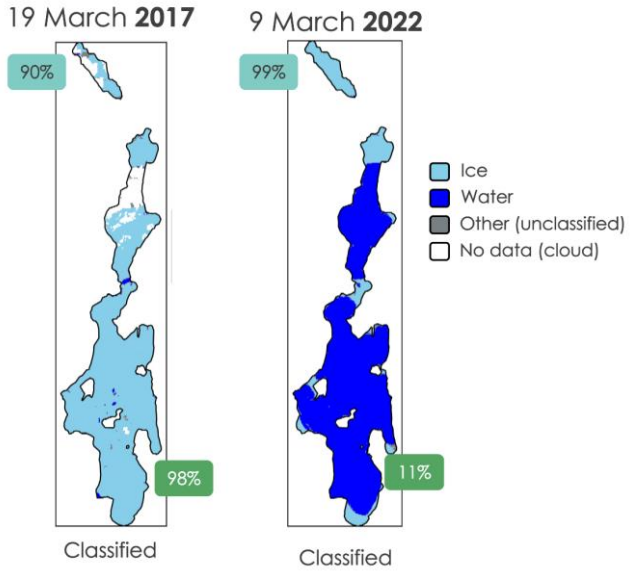

Figure G1. Calculated ice extent from classified Landsat optical scenes masked to Upper Priest Lake and Priest Lake shows 90% ice coverage of upper priest lake and 98% ice coverage of Priest Lake in March 2017; 99% ice coverage of Upper Priest Lake and 11% ice coverage of Priest Lake in March 2022.

Appendix H: *Landsat-derived Water Surface Temperature*

Table H1.
Number of Landsat-derived water surface temperature measurements for each month from the 1990-2024 (34 year) study period.

	Number of years with Landsat-derived temperature measurements	
Month	Priest Lake	Upper Priest Lake
January	8	8
February	12	8
March	15	15
April	19	19
May	26	23
June	21	21
July	30	29
August	30	28
September	29	27
October	18	18
November	8	9
December	12	12

Appendix I: *Timeline of Freezing Dates at Priest Lake*

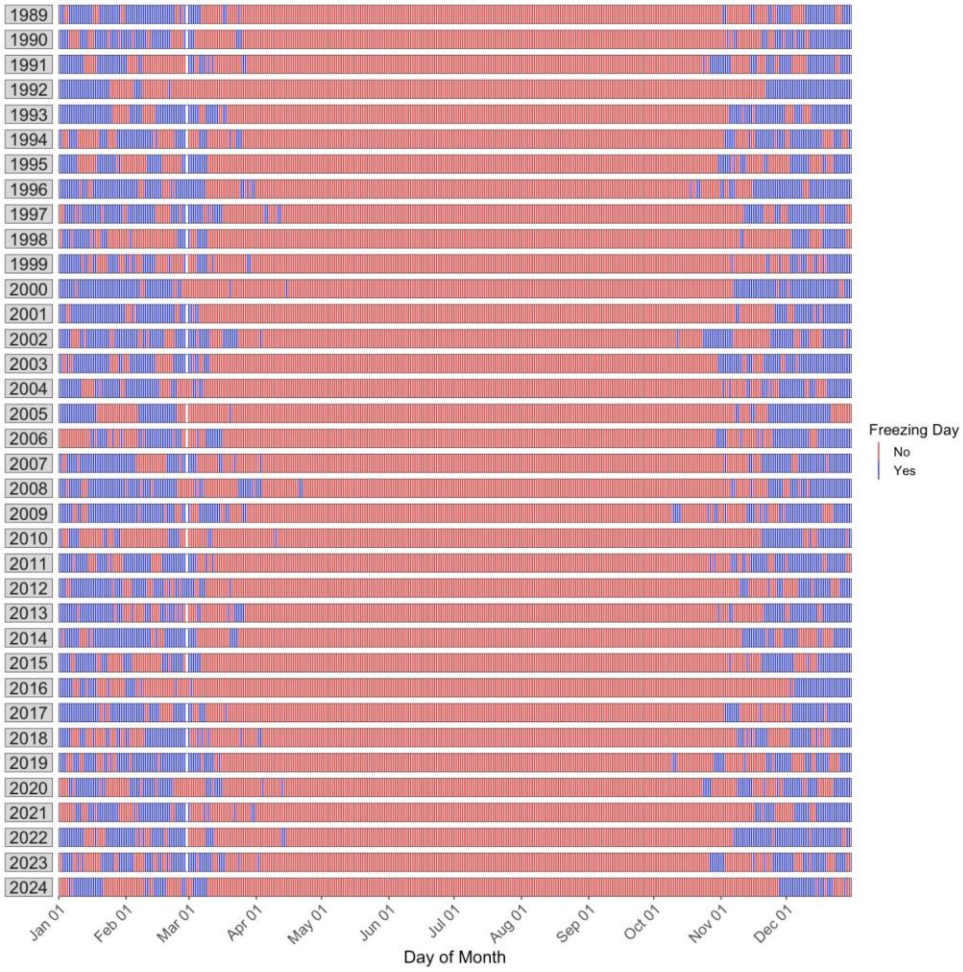

Figure I1. Timing of annual freezing dates (i.e., days with air temperature ≤0° Celsius, from PRISM) over the study period.